Master's thesis

NTNU
Norwegian University of Science and Technology
Faculty of Engineering
Department of Marine Technology

Luhao Shi

Dynamic Analysis of Semi-submersible Offshore Fish Farm Operated in China East Sea

Master's thesis in Marine Coastal Development
Supervisor: Shixiao Fu, Pal Lader
June 2019

NTNU
Kunnskap for en bedre verden

Luhao Shi

Dynamic Analysis of Semi-submersible Offshore Fish Farm Operated in China East Sea

Master's thesis in Marine Coastal Development
Supervisor: Shixiao Fu, Pal Lader
June 2019

Norwegian University of Science and Technology
Faculty of Engineering
Department of Marine Technology

NTNU
Kunnskap for en bedre verden

NTNU
Norwegian University of
Science and Technology

Dynamic Analysis of Semi-submersible Offshore Fish Farm Operated in China East Sea

Luhao Shi

MASTER THESIS

Department of Marine Technology
Norwegian University of Science and Technology

June 2019
Trondheim, Norway
Supervisor: Shixiao Fu, Pal Lader

Summary

In recent years, the aquaculture industry in China has achieved rapid development, which covers more than half of the world aquaculture production. For further development, Chinese aquaculture companies are looking for advanced farm technology available for exposed ocean condition. The semi-submersible offshore fish farm is one of the most foreseeable equipment, which is being tested in the Norwegian Sea. This thesis aims to simulate the dynamic performance of a semi-submersible offshore fish farm operated in Chinese ocean.

The farm model is constructed based on the offshore farm "Ocean Farm 1", operated by SalMar ASA. The target location of this farm is in China East Sea with a depth of around 100m. Some simplification is thus carried out at the design stage considering the actual situation in China. There are some components of the model: a main body including central pontoon, steel net frame and connectors; fish nets; mooring system.

A dynamic analysis is conducted to study the response of farm structure in both frequency domain and time domain. In order to calculate hydrodynamic properties of the farm structure, a composite model with both Morison beam and panel surface is constructed in GeniE. And simulating the composite model in WADAM, RAOs of response motion in six degrees of freedom are obtained. On the other hand, time domain analysis is executed in WASIM program, and compared with the results of frequency domain analysis. The kinetic results of the farm body acquired in WADAM are used as the input data of SIMO program to implement coupled analysis of mooring system in time domain. A catenary mooring system is modeled in SIMA to check its capability of keeping position in ultimate sea states.

For all of the simulations carried out in SIMO program, the mooring lines presented to be capable of withstanding the hydrodynamic loads from waves and currents. This thesis compares the results of motion under various environment conditions. It indicates that current dominates drift motion of the farm compared with wave drift force. However, when considering the oscillation motion of structure, wave force comes to be the main factor. Due to the symmetry of farm structure, wave from different directions only result in slight difference, and the effect of misalignment of wave and current also shows to be insignificant.

Furthermore, mooring systems with various pre-tension are tested in the same environment. The consequences of simulation verify that the pre-tension of mooring line has a significant effect on the drift of floating farm body. With the increasing of mooring line pre-tension, the performance of mooring system can be enhanced. Finally, the simplified quasi-static mooring system in WASIM is compared with the catenary mooring system in SIMO. And it illustrates the influence of nonlinear effects: the results from SIMO are less

in accordance with wave motion.

Preface

This master thesis is carried out for accomplishing my master program in Marine Coastal Development at Norwegian University of Science and Technology (NTNU). It is a summary of my study from January to June 2019.

This master thesis studies about the dynamic response of semi-submersible offshore fish farm structure in Chinese ocean. I am quite proud and pleasant for finishing such a research regarding dynamic analysis. I did make my great efforts on finishing the project and learn a lot during the process. It is of great certain that I will benefit from it all my life.

The thesis is finished under the supervision of Prof. Shixiao Fu and Prof. Pal Lader at the department of Marine Technology, NTNU. I would like to thank them for their instruction and great help during the process. They gave me guidance and feedback when I was struggling with problems.

I would also like to thank Carlos Eduardo for his providing software and guidance on SIMA. And I also need to thank Dr. Zhiyu Jiang for his help when I am modelling in SIMO program. Moreover, I want to thank Dr. Youwang Xu for his suggestion and adjusting my thesis writing. Finally, I want to appreciate my parents and friends for their support on finishing this master program.

Tondheim, June 2019

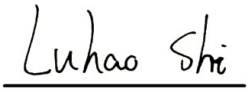

Luhao Shi

Table of Contents

List of Tables

List of Figures

Abbreviations

WMO	=	World Meteorological Organization
ITTC	=	International Towing Tank Conference
EC	=	Environment Condition
RAO	=	Response Amplitude Operator
DNV	=	Det Norsk Veritas
TD	=	Time Domain
FD	=	Frequency Domain
PM	=	Pierson-Moskowitz
JOSWAP	=	Joint North Sea Wave Project
FEA	=	Finite Element Analysis

Chapter 1

Introduction

1.1 Background

With the increasing of population, producing sufficient food comes to be a main challenge over the world. Aquaculture, with its own advantage, is one of the most promising food industry to face the problem. According to the statistic of the World Bank, 62% of seafood will come from aquaculture in 2030. Because the yield of fishing industry keeps stable, even slightly decreased in recent years, while the demand of fishing is increasing rapidly. It is foreseeable that the fishing resource available for utilization will continually suffer a large reduction due to over-exploitation (Bjelland et al., 2015). And therefore, the aquaculture is being rapidly developed for more production as shown in Fig. 1.1.

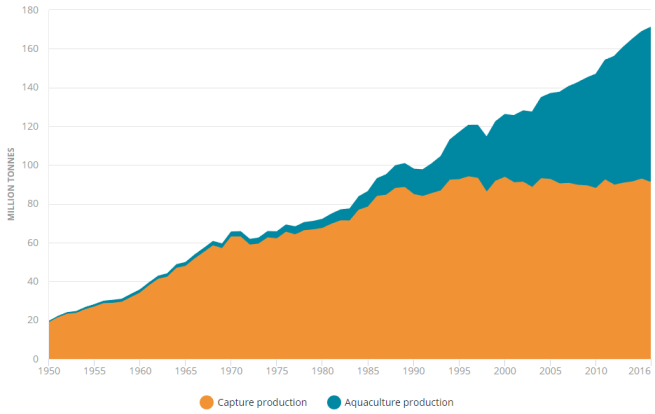

Figure 1.1: World production of fishery and aquaculture from 1950 to 2016 (FAO, 2018)

In the last decades, the fish farm for aquaculture normally locates near the coast or somewhere sheltered. With the development of aquaculture industry, the location available for fish farm is less and less. Furthermore, with the consideration of environment, the density of farming should be limited. Some of governments are restricting the breeding quantity of fish farm.

In Norway, permission from government is necessary for farming at coastal area. The permission is quite limited and expensive leading to a potential challenge of further increasing of production. Therefore, utilizing the exposed location becomes one of the feasible ways to overcome the problem. Since the existed fish farms are designed for coastal deployment, incapable of withstanding severe ocean condition, the industry is making efforts to explore new technology for offshore farming. A lot of concepts have been carried out, in which some of them are being tested.

China, with the world largest population, produce nearly 62% of world aquaculture yield. It is also the world largest exporter of fish. However, nearly all of the fish farms in China are distributed along the coastal region, and vulnerable to severe weather condition like typhoon. In addition, with the development of heavy industry, the polluted environment is becoming a potential serious threat for aquaculture.

Therefore, Aquaculture company in China is searching for farms available to withstand severe weather condition as Norwegian industry did. There are some concepts from Norwegian industry potential for implementing in Chinese ocean. Semi-submersible offshore fish farm is one of the most foreseeable equipment, which has been applied to test in the Norwegian sea as shown in Fig. 1.2.

Figure 1.2: Configuration of Norwegian offshore fish farm (Tnset, 2017)

1.2 Fish Farm Overview

The existing fish farm are mainly built up with plastic pipe and nets. The plastic farms are developed since 1980s. In recent years, there are limited innovation on designing such kind of farms. It is normally in a shape of circular with two or three floating collars as shown in Fig. 1.3.

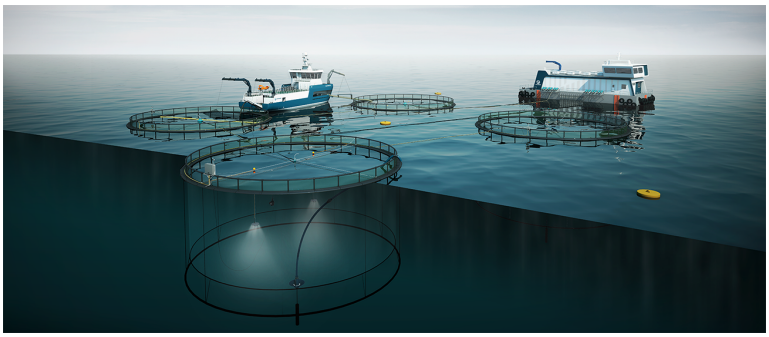

Figure 1.3: Configuration of plastic fish farm (Aqualine, 2019)

The advantage of these farms is that the materials used for construction are flexible high-density polyethylene with no hinge or steel, which makes them more sustainable to the fatigue from currents and waves. In addition, utilization of plastic leads to less consumption than other steel structure. However, when it comes to ultimate sea states, the fish nets

are vulnerable to heavy current and high wave condition. The lifting effect from current may also reduce the volume of fish cage resulting low fish welfare. The plastic fish farms are therefore only suitable for operation at sheltered region.

For offshore fish farm technology, apart from the concept introduced above, there are some other concepts, such as submersible fish cage, vessel-shaped fish farm and egg-shaped fish farm. The configuration of these fish farm are listed as following Fig. 1.4. Concept like vessel-shaped farm has been studied by Dr. Lin Li regarding the dynamic performance of the structure (Li et al., 2018). And some of them are still at the stage of designing or verification. The advantage of these farm structure comes from its capability of withstanding high sea states and much larger capacity. Both government and industry are looking forward to putting them into use.

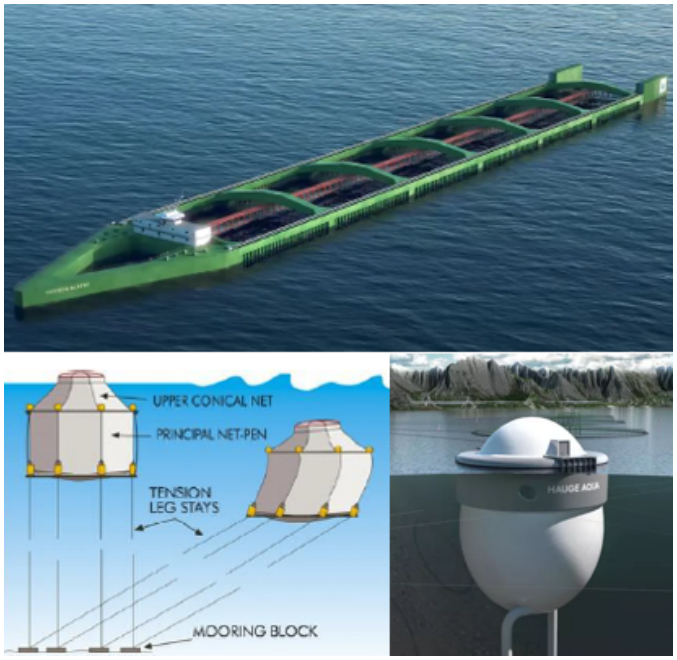

Figure 1.4: Configuration of vessel-shaped fish farm (top), submersible fish cage (left) and egg-shaped fish farm (right) (Terazono, 2017; Refamed, 2015; Nordlaks, 2015)

1.3 Motivation and Objective

The motivation of this thesis is to study the feasibility of semi-submersible offshore fish farm in Chinese ocean. The dynamic response of a farm model will be analyzed based on Chinese ocean condition. The analysis is going to be carried out in both frequency and time domain. Numerical simulation program such as ABAQUS, WADAM, WASIM and SIMO will be used to conduct the calculation.

The model is constructed referring to the design of offshore fish farm ”Ocean Farm 1”. There are some simplification implemented at the design stage considering the actual situation in China. The model are separated to several parts: main body including central pontoon, steel net frame and connectors; fish nets; mooring system. Fig. 1.5 presents the configuration of the model, where the fish nets are attached to the out frame but invisible here.

In the real condition, both operational condition and ultimate condition are important for studying the behaviour of offshore structure. However, due to time limitation, in the present research, the simulation is limited to 7 environment conditions, where only extreme weather conditions are included.

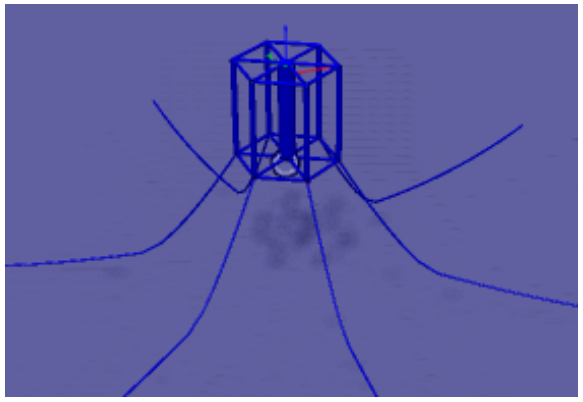

Figure 1.5: Configuration of semi-submersible offshore fish farm model

Chapter 2

Theory

2.1 Wave and Current

In the real condition, offshore structures are generally exposed to several environmental loads, such as current, wave and wind. Whereas the structure in this thesis is semi-submerged with low sensitivity to the wind loads, the discussion of the environmental loads is restricted to wave and current.

Normally, wave induced loads are regarded as the most significant loads on a floating structure, which may lead to large deformation and response motion. Wave activity is caused by wind blowing through the ocean surface, and is thus highly depended on the action of wind. In addition, the interaction between waves can also exchange the wave energy, leading to a higher wave. In order to study the features of wave and their effects on the offshore structures, some simplifications and theories are developed to model the wave action.

2.1.1 Regular Wave

The modelling of wave can be divided as regular wave and irregular wave. For regular wave, it is assumed to propagates with the same configuration permanently, which can be described by sine (or consine) function as shown in Fig. 2.1 and Eq. 2.1. It is hard to describe the real sea states by regular wave, but usually useful in studying the response motion of structure in a specific condition. To specify a regular wave, wave amplitude a, wavelength λ, and wave period T are needed. The function of wave motion can be presented as:

$$\eta(x,t) = a\sin\left(\frac{2\pi}{T}t - \frac{2\pi}{\lambda}x\right) \tag{2.1}$$

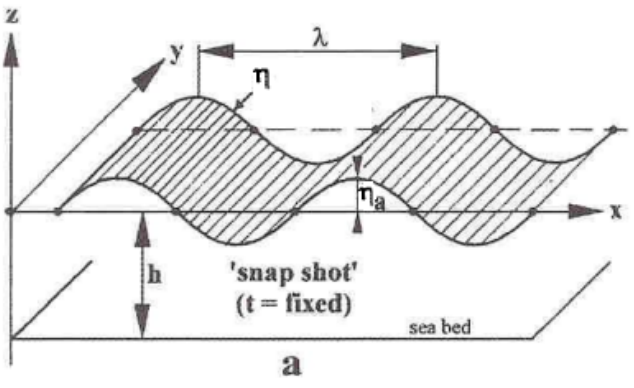

Figure 2.1: Configuration of regular wave (De Jong, 2018)

Where t and x represents the given time and location depth respectively, and η is the wave elevation. For a regular wave, the phase velocity v represents the velocity of propagating

fronts, which is related to the wave length λ and wave period T expressed as

$$c = \frac{\lambda}{T} \tag{2.2}$$

Wave number k represents the number of complete wave cycles per electromagnetic field as shown in equation 2.3, and thus equation 2.1 is sometimes written as:

$$k = \frac{2\pi}{\lambda} \tag{2.3}$$

$$\eta(x,t) = a\sin(kx - \omega t) \tag{2.4}$$

2.1.2 Irregular Wave

In a real sea state, regular wave is normally too simple to represents the wave condition precisely. Instead, the irregular wave would be a more suitable option to describe the motion of waves. Actually, irregular wave can be regarded as a superposition of sinusoidal wave components (regular wave) with different wave amplitudes and periods as shown in Fig. 2.2. According to the graph, The expression of irregular wave can be writen as:

$$\zeta = \sum_{j=1}^{N} A_j \sin(\omega_j t - k_j x + \varepsilon_j) \tag{2.5}$$

Where ε_j is a random phase independent with other parameters. Wave number k_j and wave period ω_j is related by dispersion relation as conducted above. The amplitude of regular wave components A_j normally follows a distribution like Rayleigh distribution and Gaussian distribution. The wave spectrum is formed through equation:

$$\frac{1}{2}A_j^2 = S(\omega)\Delta\omega \tag{2.6}$$

Where $\Delta\omega = \omega_j - \omega_{j-1}$.

A sea states is usually divided by wind sea and swell. While the wind sea represents the waves generated by winds in the local area, swell is normally a series of waves formed from far field. Swell waves, as a series of surface gravity waves, can propagates for a long distance and rarely affected by the local winds. Therefore, when the environment condition consists of both wind sea and swell, the wave normally presents to have multi directions. And it could be the most unfavorable condition for an offshore structure.

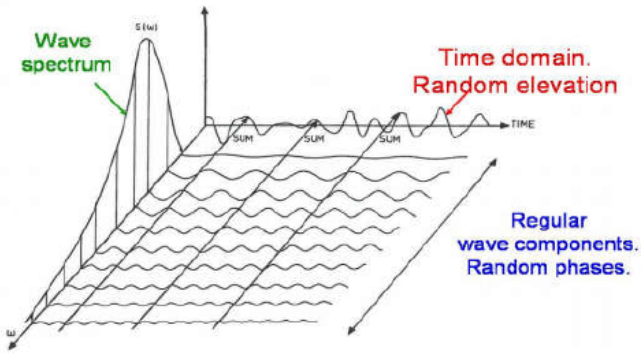

Figure 2.2: Configuration of irregular wave and wave spectrum (Greco, 2012)

2.1.3 Wave Spectrum

Wave spectrum are used for describing the distribution of wave energy in relation with wave period. For a specific area, the real wave condition can be represented by an idealized wave spectrum. In recent years, there are many wave spectrum developed according to the statistics from real sea states. And some researches were also carried out to study the similarity of the idealized wave spectra with real spectra in specific ocean (Zhu Yanrong, 1995).

Pierson-Moskowitz (PM) spectrum and JONSWAP spectrum are two of the most famous wave spectra for analysis of ocean engineering in North Atlantic. PM spectrum is developed by Pierson and Moskowitz in 1964, and modified later, which is recommended by 15th ITTC for fully-developed sea. Fully-developed sea is assumed to be that the sea condition has been blew by wind for a long period (around ten thousand wave periods) leading to a equilibrium between wind and wave. The PM spectrum is in form of:

$$S(\omega) = \frac{\alpha g^2}{\omega^5} \exp\left(-\beta \left(\frac{\omega_0}{\omega}\right)^4\right) \tag{2.7}$$

Where ω is the wave period, α and β are constants, $\omega_0 = g/U_{19.5}$ and $U_{19.5}$ represents the wind velocity at a height of 19.5 m above the water surface.

Based on PM spectrum, researchers extended the study according to the statistics in Joint North Sea Wave Project, where JONSWAP spectrum was developed in 1973. In this spectrum, an extra factor γ^r is added compared with PM spectrum and the form becomes:

$$\begin{aligned} S_j(\omega) &= \tfrac{\alpha g^2}{\omega^5} \exp\left[-\tfrac{5}{4}\left(\tfrac{\omega_p}{\omega}\right)^4\right] \gamma^r \\ r &= \exp\left[-\tfrac{(\omega-\omega_p)^2}{2\sigma^2\omega_p^2}\right] \end{aligned} \tag{2.8}$$

Where γ is a constant taken as 3.3, σ is a spectral width parameter depending on wave peak frequency ω_p:

$$\sigma = \begin{cases} 0.07 & \omega \leq \omega_p \\ 0.09 & \omega > \omega_p \end{cases} \tag{2.9}$$

The appearance of factor γ^r is because the project shows that the real sea states rarely comes to be fully developed. Wave shows to interact with each other and tends to be even higher after a long period of wind. An enhancement is thus required for better fitting of real condition. Fig. 2.3 compares the JONSWAP and Pierson-Moskowitz spectra, where an apparent enhancement can be observed.

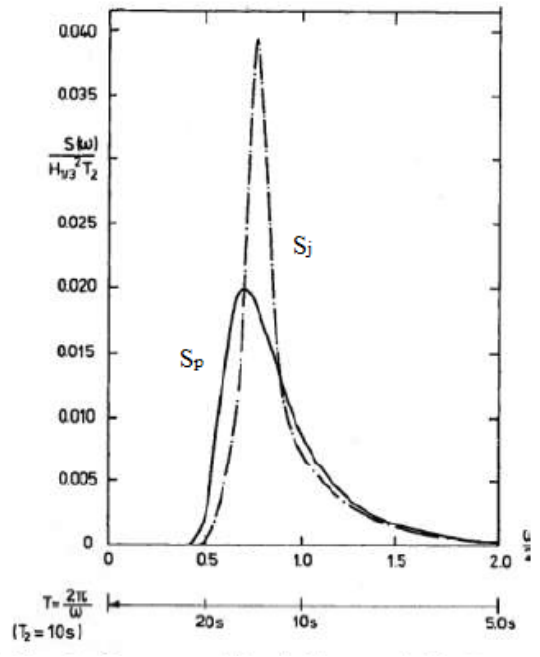

Figure 2.3: Configuration of JONSWAP spectra and Pierson-Moskowitz spectra (Greco, 2012)

2.1.4 Currents

For offshore fish farm, current appears to have a significant influence on the fish nets as well as mooring lines. The force from currents will lead to a deformation of fiber ropes and mooring chains and thus affect the response motion of the structure. It is therefore important to consider the current loads during the dynamic analysis of offshore fish farm.

The current velocity is contributed by 6 factors according to the 10th ISSC. Tab. 2.1 lists the detailed factors. In addition, the current speed also varies with the water depth and time according to the real condition. A field research is normally required according to the

geography of selected location. For numerical simulation, however, the currents are usually simplified as steady flow with a constant direction and velocity. And thus the current is in a function of water depth. In this thesis, a linear function is applied for modelling of currents.

Furthermore, as the current is generated by multi factors, the direction of current is not only depends on the wind. For a wind sea, the wave and current might be misalignment, which influences the loads applied on fish farms. Some environment conditions with misalignment of wave and current are carried out in coupled analysis to study this phenomena.

Table 2.1: Contribution factors of current

Current symbol	**Contribution factor**
U_t	Caused by tides and depending on location
U_w	Generated by local wind
U_s	Due to Stokes drift
U_m	Caused by ocean circulation (depends on location)
U_set	Depending on phenomena and storm surges
U_d	Due to Local density variations

2.2 Hydrodynamic Loads

For analysis of wave loads on floating structure, there are several methods applicable for calculation depending on the dimension of structure. For slender members, where viscous effects dominate the hydrodynamic loads, Morison equation shows to be more appropriate. However, when the structure dimension comes to be large, the diffraction effects could not be omitted. And in these cases, the potential flow theory would be necessary for calculation (Benitz et al., 2014).

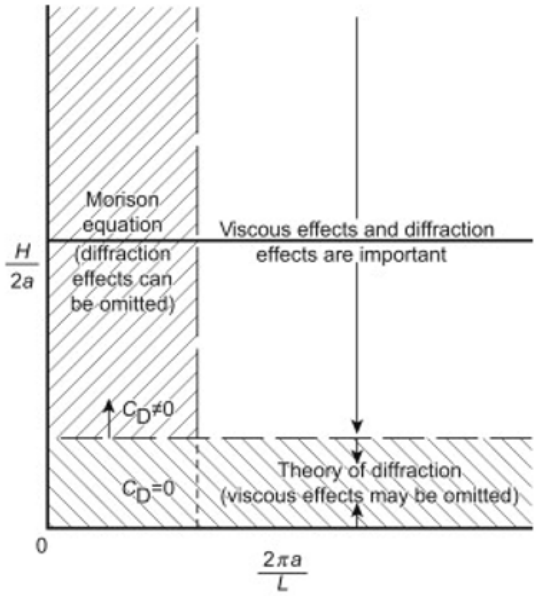

Figure 2.4: Applicable boundary for Morison equation and Theory of diffraction (Fang and Duan, 2014)

As for chosen of these two methods, empirically it can be determined by the characteristic size of structure compared with wave length and wave height. Fig. 2.4 illustrates the applicable boundary for these two methods. Normally under the same water depth, the judgement ratio could be presented by the ratio between wave height H and model characteristic length $2a$, i.e. $H/2a$, as well as the ratio of wave length L and the characteristic length, namely $a/2L$.

Normally, if $H/2a > 1.0$ and $2a/L < 0.15$, it would be capable for Morison equation to account for the wave load. On the other hand, if $H/2a < 1.0$ and $2a/L > 0.15$, potential flow theory shows to be more suitable. In this these, whereas the central pontoon is a large structure according to the judgement ratio listed above, potential flow theory will be more accurate in calculating the hydrodynamic loads on structure. However, for the slender cylinders arranged around to be nets frame and linkage, Morison equation is applicable. A composite model is thus built up in modelling of the fish farm structure.

2.2.1 Linear wave loads on large bodies

As mentioned above, potential flow theory might be the most suitable method to calculate the hydrodynamic loads on large bodies. In potential flow theory, the potential function of fluid has to be derived for calculation of loads. To conduct the wave equation, it is necessary to define the governing equation, boundary conditions and initial conditions at

the very beginning.

Assumption

Some assumptions of fluid could be made at the initial stage to simplify the flow motion. since what we concern about is the motion of sea water, it is reasonable to assume that the fluid flow is incompressible and non-viscous. The incompressible fluid means that the density will not change, while non-viscous means the shear stress among the fluid is zero (Greco, 2012). In addition, the flow is assumed to be irrotational expressed as:

$$\omega = \nabla \times U = 0 \tag{2.10}$$

Where ω represents the vorticity. And thus, the fluid velocity can be expressed in terms of velocity potential Ψ as:

$$u = \frac{\partial \varphi}{\partial x}, v = \frac{\partial \varphi}{\partial y}, w = \frac{\partial \varphi}{\partial z} \tag{2.11}$$

Governing Equation

The principles of conservation, such as conservation of mass, momentum and energy, govern the various transport phenomena of fluid flow. These conservation laws written in integral or differential form are used to solve fluid dynamic problems.

The continuity equation are partial differential equations derived according to the conservation of mass.

$$-\frac{\partial \rho}{\partial t} = \frac{\partial u\rho}{\partial x} + \frac{\partial v\rho}{\partial y} + \frac{\partial w\rho}{\partial z} \tag{2.12}$$

Where u, v, w represent the particle velocity in x, y, z direction respectively. As the density ρ of flow is constant for incompressible flow, the Eq. 2.12 comes to be:

$$\nabla * U = \frac{\partial u}{\partial x} + \frac{\partial v}{\partial y} + \frac{\partial w}{\partial z} = 0 \tag{2.13}$$

Where U is the velocity of flow. According to the expression of velocity potential in Eq. 2.11, the equation can be transferred to Laplace differential equation:

$$\varphi(x, y, z, t) = \frac{\partial \varphi^2}{\partial x^2} + \frac{\partial \varphi^2}{\partial y^2} + \frac{\partial \varphi^2}{\partial z^2} = 0 \tag{2.14}$$

Boundary Condition

When it comes to solving Laplace differential equation, boundary conditions must be applied to acquire the expression of sinusoidal wave. The boundary conditions are found according to physical reality while applying linear wave theory. There are three boundary conditions available in this case: bottom boundary condition, surface boundary condition and wall boundary condition.

For bottom boundary condition, since the seabed is not permeable to water, the vertical fluid velocity at the bottom is always zero. Therefore, sea floor boundary condition is presented as:

$$w(x, z = -h, t) = \frac{\partial \varphi}{\partial z}(x, z = -h, t) = 0 \tag{2.15}$$

The surface boundary condition illustrates the fluid is not able to flow out of water surface. There are two separate surface boundary conditions, Kinematic and Dynamic boundary condition.

Kinematic boundary condition could be explained as Fig. 2.5. When the wave motion is relatively smooth, an assumption is carried out that the fluid particle on free surface will always remain on free surface. According to the figure, the equation could be:

$$\frac{\partial \eta}{\partial t} + \frac{\partial \eta}{\partial x} u = w \tag{2.16}$$

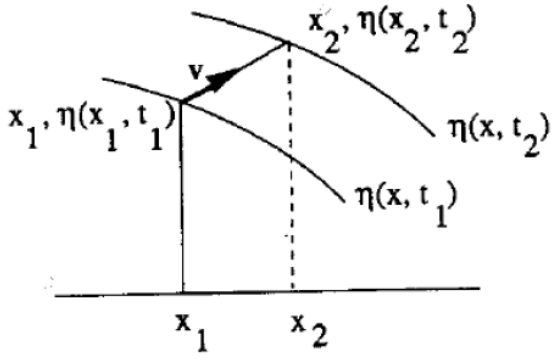

Figure 2.5: Motion of a particle on free surface

Dynamic boundary condition comes from the fact that pressure at free surface is the same with atmosphere. According to Bernoullis Equation of irrotational flow:

$$\frac{1}{2}U^2 + gz + \frac{P}{\rho} = C \tag{2.17}$$

Let $C(t) = P_{atm}/\rho$:

$$\frac{\partial \varphi}{\partial t} + \frac{1}{2}\left(u^2 + w^2\right) + g\eta = 0 \tag{2.18}$$

Combining the surface boundary conditions, and removing the nonlinear term in the formula, the equation of free surface boundary can be expressed as:

$$\frac{\partial^2 \varphi}{\partial t^2} + g\frac{\partial \varphi}{\partial z} = 0 \tag{2.19}$$

The wall boundary condition illustrates the water is not able to penetrate the body of structure, which indicates the fluid velocity normal to body surface should be the same with the velocity of structure. The expression could be derived as:

$$(\vec{v} - \vec{v}) \cdot \vec{n} = 0 \Rightarrow \frac{\partial \varphi}{\partial \vec{n}} = U_n \tag{2.20}$$

With boudary conditions listed above, it is able to solve Laplace equation $\nabla^2 \varphi = 0$ and find the velocity potential φ. In this solution, the boundary conditions are linearized according to the theory of linear wave.

Potential Flow Theory

In potential flow theory, viscous force is neglected. Instead, Froude-Krylov (FK) Force as well as Diffraction force make up the exciting force sustained by the structure. In addition, when the body of floating structure is forced to oscillate in still water with natural frequency ω, waves will be radiated from structures itself. The problem is called as radiation and subjected to loads in motion equation identified as damping, added mass and restoring force.

Under the assumption of linear wave, the hydrodynamic loads can be regarded as a superposition of exciting force and radiation force as shown in Fig. 2.6. According to the graph, the problem can be split into two parts, one is the fixed structure body interacting with incoming wave, i.e. diffraction problem, and the other is the structure oscillating without incident wave, i.e. radiation problem. But for irregular wave, it can be done by splitting the incident wave spectrum and treating as regular waves. Then the response of each component of the irregular wave is summed up as the result.

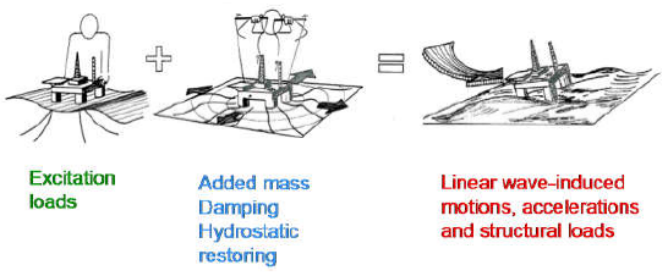

Figure 2.6: Linear hydrodynamic load (Greco, 2012)

Froude-Krylov (FK) Force

FK force is induced by the undisturbed incoming wave and calculated from a pressure field method. The method integrates the pressure on the surface of structure as Eq. 2.21. The assumption of no interference between wave and structure body is made in this theory.

$$\vec{F}_{FK} = -\int_{S_w} \rho \frac{\partial \phi_0}{\partial t} \vec{n} ds \tag{2.21}$$

Where ϕ_0 is the potential of undisturbed wave, S_w is the wet surface of the structure, $\vec{n}$ is the normal vector of body surface. According to the researches, the calculation results might not be accurate in applications, where a coefficient of force needs to be introduced for correction (Chakrabarti, 1987).

Diffraction Force

Since the structure is impermeable, the wave would be scattered by the body leading to diffraction force. For the spatial potential around the body surface, it must satisfy the impermeability condition as:

$$\frac{\partial \left(\varphi_o + \varphi_D\right)}{\partial n} = 0 \quad \forall \mathbf{P} \in s \tag{2.22}$$

Where φ_D is the potential of diffracted wave. And the diffraction load can be calculated by:

$$\vec{F}_{FD} = -\int_{S_w} \rho \frac{\partial \phi_D}{\partial t} \vec{n} ds \tag{2.23}$$

Radiation Force

Radiation force is induced by the vessel motions in six degrees of freedom. In the still water, fluid momentum is changed due to oscillation of structure leading to force acting on the body. The force can be calculated by the integration of pressure on the wet surface:

$$\tau_{rad,i} = \begin{cases} -\iint_{S_w} \left(\frac{\partial \Phi_{\text{rad}}}{\partial t}\right)(n)_i ds \quad i = 1,2,3 \\ -\iint_{S_w} \left(\frac{\partial \Phi_{\text{rad}}}{\partial t}\right)(r * n)_{i-3} ds \quad i = 4,5,6 \end{cases} \tag{2.24}$$

Where $i = 1, 2, 3$ and $4, 5, 6$ represents the freedom of the structure, namely surge, sway, heave and roll, pitch, yaw respectively, and Φ_{rad} is the potential of radiation wave.

2.2.2 Hydrodynamic Loads on Slender Structure

Morsion Equation

Morison equation is a semi-empirical formula accounting for hydrodynamic force on slender structures. It is in form of two compositions as Eq. 2.25: inertia force and drag force. The inertia force is introduced by the local flow acceleration, and the drag force is proportional to square of relative velocity between flow and body.

$$F = \underbrace{\rho V \dot{u} + \rho C_M V(\dot{u} - \dot{v})}_{F_I} + \underbrace{\frac{1}{2}\rho C_d A(u - v)|u - v|}_{F_D} \tag{2.25}$$

Where $\dot{u}$ is the flow acceleration, $\dot{v}$ is the body acceleration, u is the flow velocity, v is the body velocity, V is the volume of structure, A is the reference area, C_m is the inertia coefficient and C_d is the drag coefficient. The inertia coefficient is related to added mass coefficient C_a where it can be expressed as $Cm = 1 + Ca$. For circular cylinder, $Ca = 1$ and $Cm = 2$. Drag coefficient C_d depends on the object geometry, both skin friction and form drag must be taken into consideration. Generally, C_d is set through the Reynolds number. According to Robert. E. Randall, when drag force of a cylinder is significant, the coefficients could be selected as following Fig. 2.7 (Randall, 1997):

Stochastic Drag Linearization

In this thesis, the farm model is built up with both Morison elements and panel elements. However, Morison equation is not able to account for nonlinear loads in frequency domain. Therefore, the drag term in Morison equation has to be linearized. There are two methods available for linearization: regular wave linearization and stochastic lineariztion.

For regular wave linearization, the quadratic damping is assumed to be replaced by linear damping with the same dissipated energy. Under this assumption, wave amplitudes for each periods are needed for calculation (Shao et al., 2016). However, the stochastic linearization considering linearize the wave spectrum directly. The assumption is made that the excitation is in Gaussian stochastic process, and therefore the least square method can be applied to conduct linear damping. For frequency domain simulation carried out in

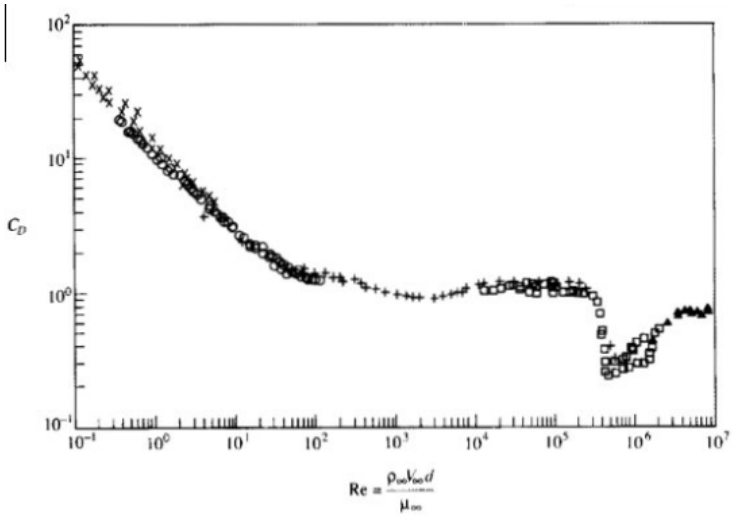

Figure 2.7: Variation of cylinder drag coefficient with Reynolds number (Randall, 1997)

WADAM program, the stochastic approach is chosen to handle the drag term in Morison equation. For a strip of dl, the drag force can be calculated as:

$$dF_D \approx \frac{1}{2}\rho C_D D\sqrt{\frac{8}{\pi}}\sigma_{|v-u|}(v-u)dl = b_v(v-u) \tag{2.26}$$

$$b_v = \frac{1}{2}\rho C_D D\sqrt{\frac{8}{\pi}}\sigma_{|v-u|}dl \tag{2.27}$$

Where $\sigma_{|v-u|}$ represents standard deviation of relative velocity, D is the diameter of model. And b_v represents the linearized damping coefficient for the strip.

With Morison equation 2.25 and Stochastic linearization equation 2.26, the Morison loads are calculated through integrating the inertia forces and linearized drag forces on each Morison elements. The motion equation of Morison elements can be presented as (Shao et al., 2016):

$$\begin{aligned}&\left(-\omega^2\left(M + A(\omega) + A_{mor}\right) - i\omega\left(B(\omega) + B_{mor}\right) + C\right)x \\ &= F_{exc}(\omega,\beta) + F_{exc,mor}\end{aligned} \tag{2.28}$$

Where β is the wave heading, A_{mor} is the added mass damping matrix introduced by Morison elements, $A(\omega)$ represents the frequency dependent added mass matrix, $B(\omega)$ represents frequency dependent damping matrix, C is the hydrostatic restoring matrix, $F_{exc}(\omega,\beta)$ represents the wave exciting force, $F_{exc,mor}$ represents the Morison exciting force.

2.3 Motion Equation and RAO

For a rigid structure floating at the sea surface, the motion equation in frequency domain can be expressed as:

$$(M + A(\omega))\ddot{x}(\omega) + B(\omega)\dot{x} + Cx(\omega) = F(\omega) \tag{2.29}$$

Where M is the mass matrix, $A(\omega)$ is the frequency dependent added mass matrix, $B(\omega)$ is the frequency dependent damping matrix, C is restoring matrix, $\ddot{x}$, $\dot{x}$, x are structure acceleration, velocity, displacement respectively, and $F(\omega)$ is exciting force.

For a nonlinear system, the equation 2.29 is not able to be solved directly. Iteration on every time step has to be applied, where a nonlinear model is needed, know as Duhamels integral. The equation 2.30 presents the form of Duhamels integral. It is in time domain, and calculates the results based on frequency dependent added mass and linear radiation damping (Naess and Moan, 2013).

$$\left(M + A^{\infty}\right)\ddot{x}(t) + \int_0^t \kappa(t-\tau)\dot{x}(\tau)d\tau + Cx(t) = F(t) \tag{2.30}$$

According to Eq. 2.29, for an certain external force with various frequencies, a serious of response of model can be computed. The relation between force and response is expressed as Response amplitude operator (RAO) in frequency domain. RAO represents a transfer function between amplitude of excitation and structure response (Veritas, 2010).

Each RAO can present the hydrodynamic property of the structure for one degree of freedom. And therefore, six RAOs in different degree of freedom can be used to express the response of structure under a certain external load.

2.4 Finite Element Method

The essence of Finite element analysis (FEA) is a numerical method in which a continuous structure is divided into finite substructures. These substructures are known as elements, and the process is called discretization. In this way, the structure with infinite degrees of freedom is modeled with elements having finite degrees of freedom. As long as the element size is small enough, the deformation of elements can be computed by low-order polynomials under acceptable approximation.

In this thesis, under the assumption of rigid body, the elastic effect of farm main structure is ignored. The kinetics of the main body is import from the results of Frequency domain analysis in WADAM. However, when considering the calculation of fish nets and mooring lines, finite element method would be of great importance. In calculation, the net or line

structure is divided into small elements, and the mass, damping and stiffness properties for all of these elements can be expressed by a global matrix. The nonlinear motion equation of the structure is solved based on this matrix as shown in following equation:

$$\left(M^s + M^H\right)\ddot{r}(t) + C^s\dot{r}(t) + K^s(r(t)) = R^{EXT}(r(t), \ddot{r}(t)) \tag{2.31}$$

Where R^{EXT} represents the loads matrices suffered by the structure, including hydrodynamic loads and forced displacement, velocities, acceleration from the coupled structures. Whereas only simplified dynamic analysis is available in SIMO, only drag force is accounted in hydrodynamic loads. The nonlinear equation 2.31 in SIMO can be solved through modified Euler method, 3rd-order Runge-Kutta-like method or Newmark-Beta predictor-corretctor method. This thesis applies Newmark-Beta method for numerical integration on each time step (Marintek, 2017).

2.5 Mooring System

The mooring system is normally composed of mooring lines, anchor and connectors. Functionally speaking, the mission of a mooring system is to restrict the structure or vessel in a desired position for safety consideration. The main jobs of mooring lines are to control mean offset, low-frequency motions and diminish wave-frequency motion (Larsen et al., 2015).

While designing of mooring system, the deployment periods must be taken into consideration. A mobile mooring system usually stays at a specific site less than 5 years, which means that mooring lines and anchors are designed adaptive to installation, repetitive handling and retrieve. However, for permanent mooring like semi-submersible platforms, the anchors are generally not retrieved. Therefor, the system are designed focus on the strength and fatigue requirements (Larsen et al., 2015).

2.5.1 Categories of Mooring System

The mainstream mooring system can be separated as two main categories: turret mooring and spread mooring system. It is of great importance to figure out the performance characteristics of the mooring systems, since it may affect the structure operation and motion response. Fig. 2.8 shows the configuration of these two kinds of mooring system.

For turret mooring system, it is usually operated on vessels like FPSO, because it allows vessels rotate around the turret according to weather condition. The feature of turret enables structure to withstand minimal environment condition. There are mainly three types of turret: Internal turrets; Disconnected internal turrets; External turrets.

Spread mooring system is the one used in this thesis. It has fixed orientation, and thus would be suitable for operating sites with less severe weather condition. The mooring

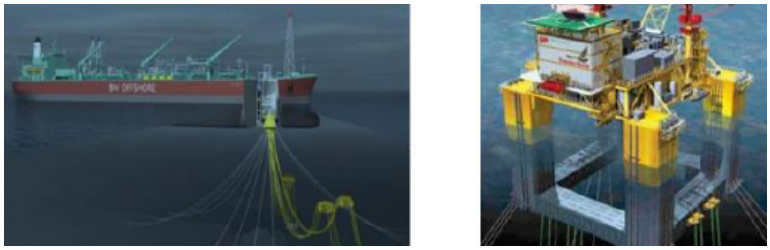

Figure 2.8: Configuration of turret mooring (left) and spread mooring system (right) (Larsen, 2014)

lines are connected to multi points on the vessel instead of turret, which is considered to be less costly than former one.

2.5.2 Mooring System Arrangement and Components

Catenary mooring, Taut mooring and catenary mooring with buoyancy elements are the most common arrangement in mooring systems. The components of these arrangements are listed as following Tab 2.2. The main difference among these arrangements are that while catenary mooring anchor only resists horizontal force, taut mooring is able to withstand both horizontal and vertical force. Thus, catenary system comes to be failed when there are lifted force applied on the anchor.

Table 2.2: Components of mooring arrangements

Arrangement type	**Components**
Catenary mooring	Chain-steel wire-chain
Submerged weight	Chain-synthetic fiber ropes-chain
catenary mooring with buoyancy elements	Chain-steel wire-buoy-steel wire-chain

Fig. 2.9 shows the configuration of different mooring arrangements. According to the graph, it is obvious that the resisting force of taut system comes from mooring line elasticity whereas catenary system uses line weight to resist the motion of vessel.

The most common mooring line types for floating structures are Steel linked chain and wire rope. Chain can be studless or stud-link, depends on the mooring periods. Traditionally, the stud-link chains with better installation and retrieval performance are used for mobile mooring system such as FPSOs. In contrast, the studless chains have higher stiffness and longer fatigue life, which would be preferred to be operated on semi-submersible platforms with permanent mooring system (Larsen, 2014). As the semi-submersible offshore fish farm will be deployed at the location for the whole life period, studless chains come to be better choice.

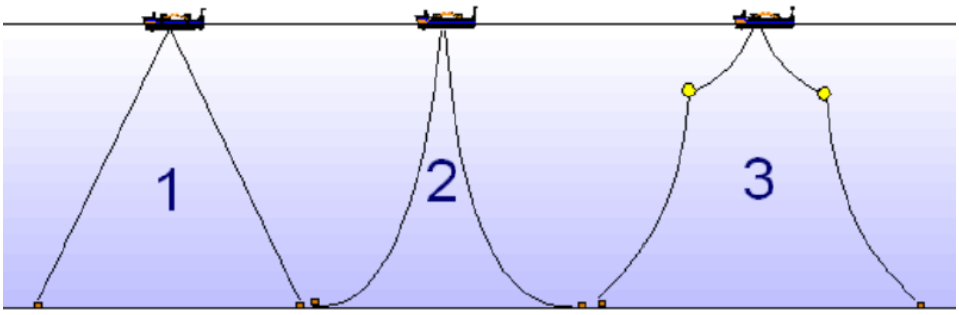

Figure 2.9: Configuration of mooring arrangements (Larsen, 2014)

Steel wire ropes are normally lighter than chains, and used as connecting elements among chains, buoy and shackles for excellent fatigue property. Synthetic fiber ropes could be even lighter but perform a higher elasticity. The advantage of fiber is that it reduces the loads with relatively high tension limits (Larsen, 2014).

2.5.3 Dynamic Tension Computation Model

The analysis of catenary mooring line model in SIMO program is either quasi-static or simplified dynamic accounting for drag force effect. In order to increase the accuracy of simulation results, simplified dynamic analysis is applied. However, with dynamic effects of mooring line velocity and acceleration, the line tension might vary from the results of quasistatic calculation of structure motion (Marintek, 2017).

Dynamic tension computation model is thus used to account for this effect. The model is developed by Larsen and Sandvik based on some assumptions (Larsen, 1990):

1. Only tangential motion of the top end has effect on dynamic tension.

2. The shape of dynamic motion due to tangential excitation is equal to the deformation of static line geometry.

3. Neglecting the mass force of mooring line.

4. The elastic elongation of mooring line is determined by quasistatic analysis

Fig. 2.10 illustrates the dynamic tension computation model, in which the moment equilibrium regarding point P yields:

$$\int_0^S \left| \mathrm{d}\overrightarrow{f_c} \times \vec{r} \right| \mathrm{d}l = aT_{DC} \tag{2.32}$$

Where T_{DC} is the tension caused by drag force and calculated as:

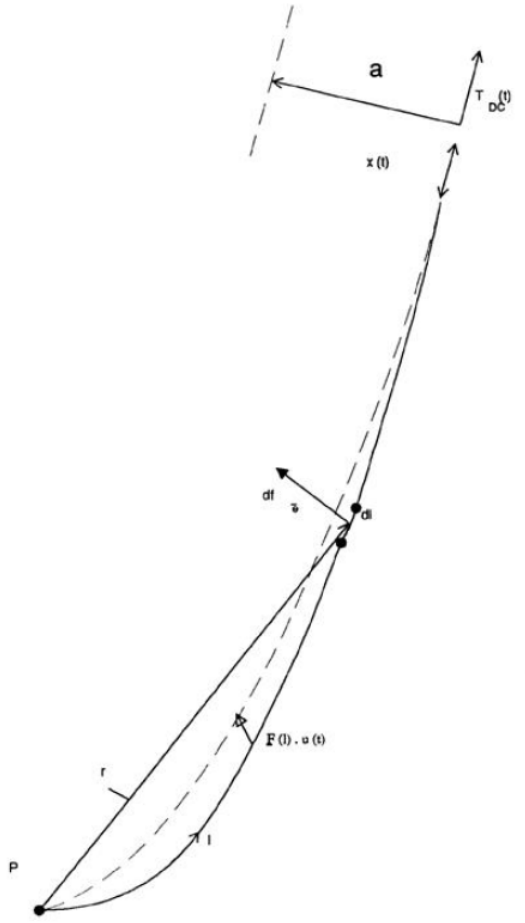

Figure 2.10: Dynamic tension computation model (Marintek, 2017)

$$T_{DC} = k^E(x - u) - k^G u \tag{2.33}$$

The line motion equation is then given by:

$$c^* \dot{u}|\dot{u}| + k^* u = k^E x \tag{2.34}$$

Where c^* is generalized line damping, k^* is generalized line stiffness, k^E is the axial line stiffness, k^G is the geometric catenary stiffness, u is the displacement of the mooring line, $\dot{u}$ is the velocity of the mooring line, x is tangential motion excitation of the top end (Marintek, 2017).

2.6 Fish Nets

Fish nets, for the main function in aquaculture, are used to trap fish in a fixed area. At the meantime, current should be able to penetrate the nets to provide sufficient fresh water and oxygen. In some farming region, they also need to prevent fish from predators like shark. While the thick net rope decreases the possibility of fish escaping crisis, it may lead to less current flow through the cage and more material expense. And thus the manufacturing of fish nets largely depends on the farming site and environment condition they must endure. There should be a balance between net thickness and costs. A concept of solidity ratio is then forward to represent the permeability of the fish nets. It is defined as the ratio of net area and frame area. For a square shaped net, Sn can be expressed as:

$$S_n = \frac{2d}{\lambda} - \left(\frac{d}{\lambda}\right)^2 \tag{2.35}$$

Where λ represents the mesh size and d could be rope diameter as shown in Fig. 2.11. It is notable that the solidity ratio might be changed by marine growth and fouling when the nets are submerged in water for a long period. The fouling degree depends on the location, nets material, fish species and etc. And considering the ultimate state, the effect of fouling should be estimated by increasing solidity ratio (Lader and Fredheim, 2006).

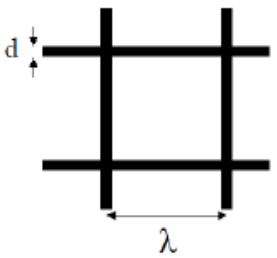

Figure 2.11: Parameters of fish nets

Nowadays, nylon nets with low solidity ratio are the most common choice for fish cages in aquaculture. The nets are normally positioned by floating collars and bottom weights, which is a highly flexible structure. When encountering with currents, the properties of nets make the flow go around and partly through the structure as shown in Fig. 2.12. The flexibility of cage geometry allows a large deformation of nets, which in turn influence the current force acted on the structure. Thus, the challenge of nets in this form would be maintaining sufficient swimming space and keeping fish welfare in strong currents. This is also the main limitation for deploying fish farms in the exposed region with strong current conditions (Sunde et al., 2003).

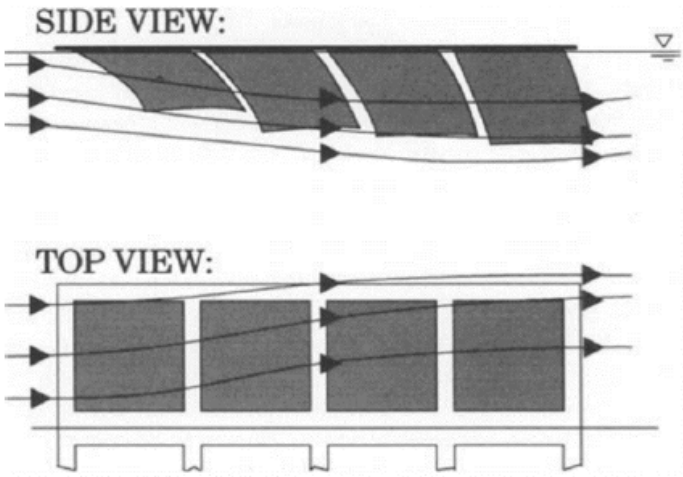

Figure 2.12: Current flow through nets and deformation (Løland, 1993)

In comparison, fish nets located in the framework of steel structure would be less flexible. A simulation is implemented in ABAQUS to check the deformation of nets. The model is constructed based on the dimension of an offshore fish farm with truss elements. The solidity ratio of nets is selected as 0.13. The results indicate that only limited horizontal deformation would be allowed. Fig. 2.13 shows that the largest displacement is less than 1.2m, where the environmental condition is: linear wave $Tp = 4s, Amp = 2m, Dir = 0deg$, constant current $Vc = 0.5m/s, Dir = 0deg$. And compared with bottom weight nets, nets in the framework would not be lifted by current force leading to less variation of attack angle.

As the deformation is negligible, fish nets for offshore fish farm in SIMO simulation could be simplified as rigid slender beams. Moreover, the number of beam elements are going to be reduced for faster calculation. A detailed discussion of simplification and sensitivity study would be carried out in the latter part of this thesis.

2.6.1 Drag and Lift Force on Fish Nets

With regard to the hydrodynamic loads on fish nets, tremendous researches have been done with both experiment and simulation. In this thesis, the mean drag and lift forces on fish nets are calculated according to equations (AKSNES, 2016):

$$F_d = \frac{1}{2}\rho C_d A U^2 \tag{2.36}$$

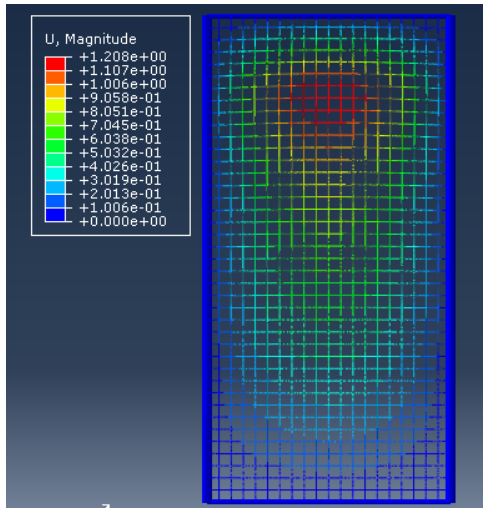

Figure 2.13: Simulation of nets deformation in truss model

$$F_l = \frac{1}{2}\rho C_l A U^2 \tag{2.37}$$

Where ρ is fluid density, C_d is drag coefficient, C_l is lift coefficient, A is the area of net panel, and U is the relative velocity vector. The drag and lift coefficients are computed according to empirical formula (Løland, 1991, 1993):

$$C_d = 0.04 + \left(-0.04 + 0.33S_n + 6.54S_n^2 - 4.88S_n^3\right)\cos\theta \tag{2.38}$$

$$C_l = \left(-0.05S_n + 2.3S_n - 1.76S_n^3\right)\sin 2\theta \tag{2.39}$$

Where Sn is the solidity ratio, θ is the attack angle, which is the angle between net normal vector and current direction. Fig.2.14 illustrates the configuration of attack angle. As the net panels are rigid beams, the attack angle of panel on each frame is fixed, depending on the frame position and flow direction (Li et al., 2018). Since Equations (2.38) and (2.39) are empirical equations, the solidity ratio Sn is limited to range 0.13 to 0.32 (Lader and Enerhaug, 2005).

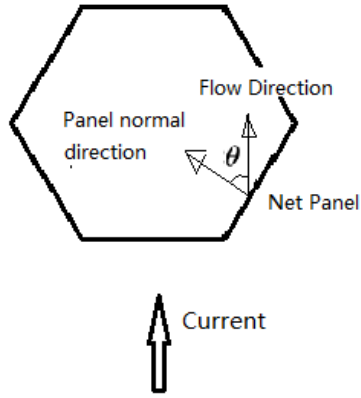

Figure 2.14: Illustration of attack angle

2.6.2 Velocity Reduction

While the permeability of nets allows the current to flow through the cage, it will reduce the velocity of flow at the meantime. Since the hydrodynamic loads on a net panel are calculated by a function of the square of flow velocity, it is of great importance to obtain the accurate velocity description on each net panel. And therefore, the velocity reduction factor is taken into account.

Velocity reduction factor $r$is defined as the ratio of velocity in the wake behind nets u and incoming flow velocity U (Løland, 1991):

$$u = rU \tag{2.40}$$

According to Løland, the velocity reduction factor can be described through net drag coefficient or net solidity ratio as shown in Fig. 2.15. In this thesis, the reduction factor is calculated through an empirical method, where $r = 1 - 0.46Cd$.

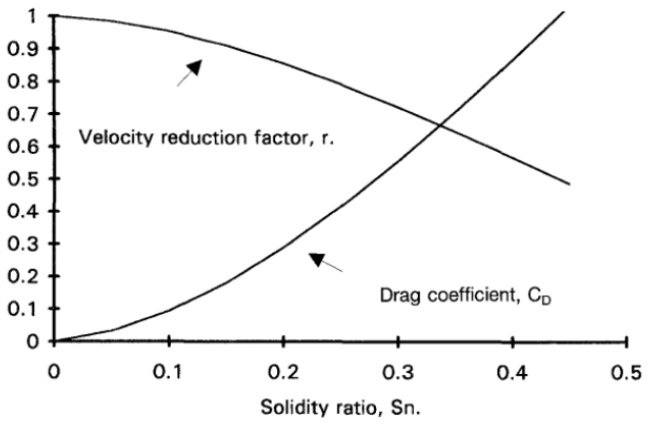

Figure 2.15: Velocity reduction factor and drag coefficient (Løland, 1991)

Apart from the velocity reduction of nets, the front panel width and distance between two net panels can also determine the flow velocity encountered by the latter nets. Setting the initial velocity $u = 0.8U$, which could be regarded as flow pass net panels with a solidity ratio of 0.17. Fig. 2.16 indicates the velocity profile behind a width of 10m net panel. It is obvious in the figure that the velocity reduction effect lasts in a long downstream. However, as the dimension of offshore fish farm is around 40m, it is assumed that the latter net panel encounters a flow velocity 90% of initial velocity behind the front panel.

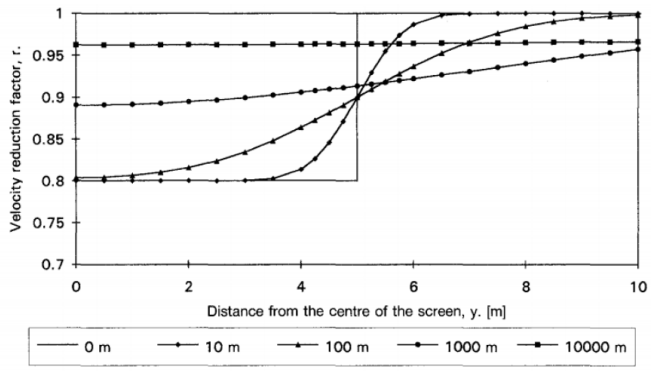

Figure 2.16: Velocity behind a net panel with 10m width and reduction factor of 0.8(Løland, 1991)

Chapter 3

Dynamic Analysis in Frequency Domain and Time Domain

Dynamic response of a structure is normally presented with frequency domain or time domain. For analysis in time domain, the response motion can be observed as a function of time. The developing phenomena in real condition are studied. Therefore, time domain is preferred in analyzing the motion in specific sea states.

However, in frequency domain, time is no longer a parameter. Motion is described by a function of frequency instead, where a transfer function of harmonic components is provided. With frequency in a wide range, frequency domain would generally be more suitable to study the hydrodynamic properties of the offshore structure. In addition, computational expense of frequency domain is much less than time domain.

In this chapter, frequency domain analysis is performed in WADAM program to investigate the uncoupled response motion of main steel body of the semi-submersible fish farm, including heave, pitch and roll. The fish farm is modeled as a rigid body with six degrees of freedom. Three wave directions and one wave spectra are chosen for fully describing the motion of the structure. In order to prove the accuracy, frequency set and panel mesh are optimized by the convergence test. The results of the analysis will be delivered to SIMA program as an input parameter of time domain coupled analysis.

Moreover, a time domain analysis is carried out in WASIM program, where the mooring system is added through anchor elements with pretension and constant stiffness. Whereas the anchor element is simplified as massless linear spring, the analysis carried out will be quasi-static coupled. The result of the simulation aims to compare with the response spectrum from frequency domain simulation.

3.1 WADAM Analysis in Frequency Domain

There are many approaches available for calculating the hydrodynamic loads on offshore structure. Computational Fluid Dynamic is, for instance, a kind of method regarded to have high accuracy. However, the cost of computational resources is too large to obtain fine results in limited time. During the early phase of structure design, engineers prefer a less computational approach, though the results are less accurate. Therefore, SESAM suite of program is developed by DNV GL to acquire hydrodynamic performance of vessels and offshore structures. WADAM is a program in SEASAM for wave loads calculation (HYDROD, 2006).

The environment condition of this simulation is set as Fig. 3.1. The water depth of the location is 100m, and water density, air density, gravitational acceleration and kinematic viscosity are included as input parameters. Whereas the response motions may vary with different wave direction, three wave directions are applied in this simulation, i.e. 0, 45, 90 degree.

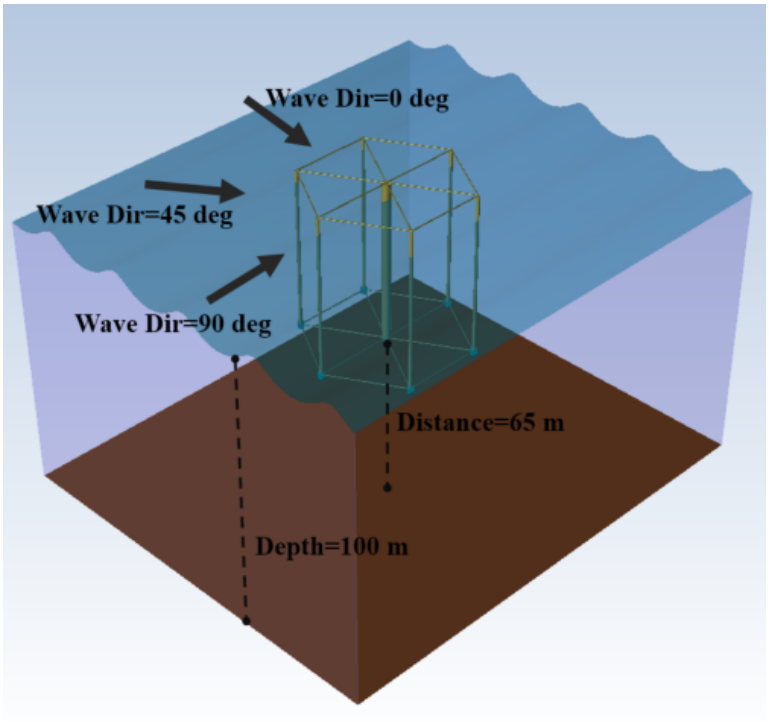

Figure 3.1: Wave directions and water depth of the fish farm

3.1.1 Composite Model

As mentioned above, the main body of fish farm structure is designed to composite both large volume structure and slender beams. For the pontoon at the centre of the farm, potential flow theory is applied, and therefore, it is constructed with panel model. Panel model is modeled based on quadrilateral panels, which represents the surface of the structure. Each of the panels corresponds to a flow element. According to the potential flow theory, the velocity potential is derived in this element from the Laplace equation. The wave force is then available on each panel. And hydrodynamic loads comes from summing up of these forces. (HYDROD, 2006). The panel model of pontoon is meshed with 1 m panel according to the requirements given in DNV-RP-C205 (Veritas, 2010):

1. The smallest wavelength analysed should be at least 6 times of diagonal length of panel mesh.

2. Geometry with abrupt changes, such as corners, should be applied with fine mesh.

3. If both sides of a wall structure are applied with wet surface, the mesh is supposed to be smaller than 4 times of the model thickness.

4. The modeled structure is supposed to be similar with real structure regarding the geometry and wet surface.

On the other hand, the net frame cylinders and connective beams are modeled through Morison beams, where Morison equation can be applied. Each of the cylinder is divided into ten Morison beams accounting for the inertia and drag force on the beams. The geometry of the beams is specified as Fig. 3.2. In addition, added mass coefficient, as well as drag coefficient, are indispensable inputs in calculating hydrodynamic force with Morison equation.

Added mass coefficient in Morison equation accounts for the inertia term of wave force. For a circular cylinder, it is normally taken as $C_a = 1$. Drag coefficient is a dimensionless parameter for calculating drag force. The selection of drag coefficient is generally related with Reynolds number, which can be determined as the following equation:

$$Re_{crest} = \frac{u_{\max} \cdot D}{\nu} \tag{3.1}$$

Where Re_{crest} represents the Reynolds number in wave velocity u, D is the characteristic diameter of beam, ν is the kinematic viscosity of sea water. With the parameters listed in Tab. 3.1, the Reynolds numbers is found to be $Re = 9 * 10^5$ for net frame beams and $Re = 3.4 * 10^5$ for connective beams. According to the relation mentioned in the theory chapter, this thesis applies $C_d = 0.7$ and $C_d = 0.5$ on net frame and connective cylinders respectively (Randall, 1997).

Table 3.1: Dimension of cylinders and environment data

Parameter	**Symbol**	**Unit**	**Value**
Kinematic viscosity	ν	(m^2/s)	10^{-6}
Frame cylinder diameter	D_{frame}	(m)	0.8
Connective cylinder diameter	$D_{connector}$	(m)	0.3
Gravitational acceleration	g	(m/s^2)	9.81
Wave height	H	(m)	4
Wave frequency	ω	(rad/s)	0.79
Water depth	z	(m)	100

Fig. 3.2 illustrates the detail dimension of farm model, which is built up by modelling tool in GeniE, SESAM. GineE is a design and analysis tool developed by DNV GL for fixed or floating offshore structure.

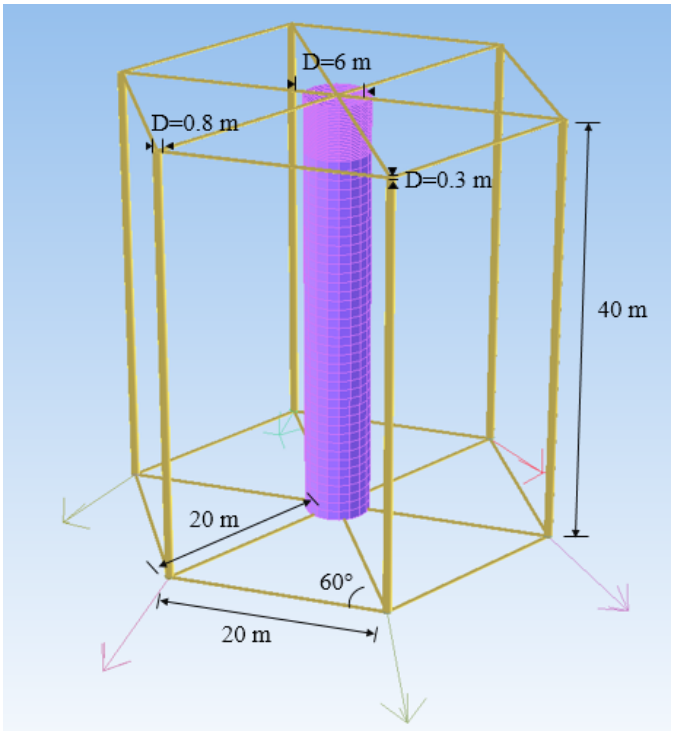

Figure 3.2: Detailed dimension of fish farm body

3.1.2 Wave Spectrum

In frequency domain analysis, Bretschneider wave spectrum is added in simulation, which could also be regarded as modified PM spectrum. Bretschneider wave spectrum is developed mainly for fully developed sea condition. Since both panel model and Morison model are included, stochastic drag linearization must be applied on the wave spectrum. For setting up of the wave spectrum, two essential input parameters, namely significant wave height Hs as well as wave period T, should be assigned. Considering the environment condition discussed in next chapter, the parameters are selected as $Hs = 4m$, $T = 10s$. Fig. 3.3 presents the configuration of wave spectrum with these inputs.

3.1.3 Frequency Set

A frequency set determines the accuracy of the final results and effects the computing time. In this analysis, a frequency set with same frequency step is applied at the initial stage to find out the area of peak amplitude roughly. And then a more concentrated frequency is added to the location around amplitude peak, which is the area of interest. The process could be done using the input function in WADAM. Normally for computation of frequency domain, a frequency set of at least 30 frequencies at interest area is required in

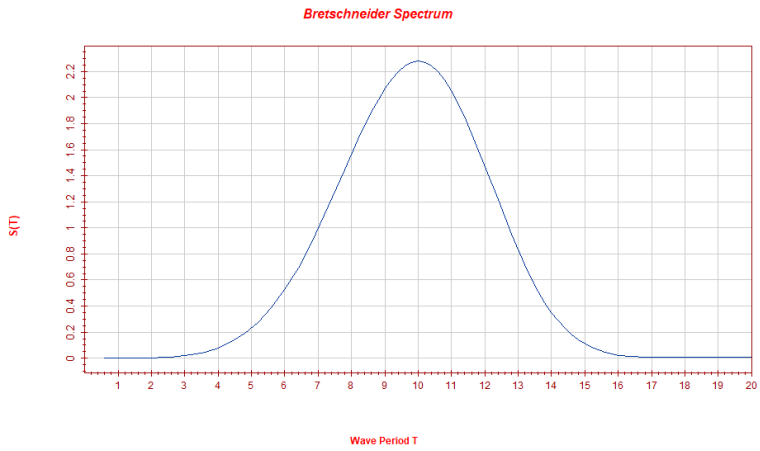

Figure 3.3: Bretschneider wave spectrum

WADAM analysis according to DNV-RP-C205 (Veritas, 2010). The results of frequency domain analysis compare the influence of frequency sets. The final frequency step is set to be $0.02rad/s$ at the most interest area in this thesis.

3.1.4 Hydrodynamic Results

In order to have sufficient accuracy for further analysis in time domain, a sensitivity study of frequency set is carried out. The direction of the wave is set to be $0deg$. With increasing density of frequency set, resulted heave RAOs of fish farm structure is presented as Fig. 3.4.

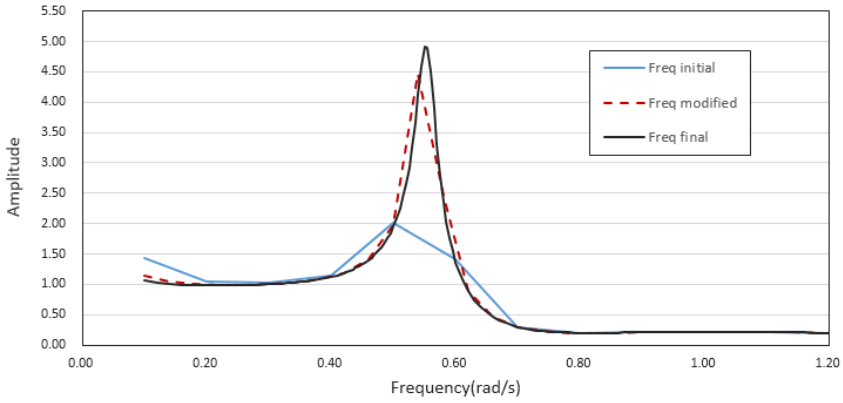

Figure 3.4: Comparison of heave RAOs with different frequency set

At the initial stage, a linear frequency set with a step of $0.1rad/s$ is applied. It is observed that the interest area locates at $0.4 - 0.7rad/s$. However, due to the limited step dense, the peak amplitude of RAO is quite smooth means insufficient accuracy.

In the latter simulation, the density of frequency set is raised to $0.04rad/s$ with a linear spread. And in the final one, the frequency step in the range of $0.4 - 0.7rad/s$ is further reduced to $0.02rad/s$. Fig. 3.4 compares the difference of resulted RAOs. It is obvious that the result of the final frequency set is similar to the modified one but still shows to have a larger peak amplitude. And therefore, the frequency set is chosen as the third simulation.

For frequency set in other motions and other wave directions, the RAO results are listed in appendix A. Tab. 3.2 lists the maximum amplitudes of different motions and wave directions. Concerning the frequency density, the final amplitudes of RAOs are increased by 243%, 12%, 12% for heave, pitch and roll respectively. It indicates that sufficient measurements are important in finding peak amplitude of RAOs.

Table 3.2: Maximum amplitudes of RAOs in different motions and wave directions

Motion	Frequency set	Direction 0 deg	Direction 45 deg	Direction 90 deg
Heave	Initial	2.02	2.22	2.03
	Modified	4.68	4.70	4.69
	Final	4.91	4.91	4.93
Pitch	Initial	0.09	0.07	0
	Modified	0.09	0.06	0
	Final	0.11	0.08	0
Roll	Initial	0	0.07	0.10
	Modified	0	0.07	0.011
	Final	0	0.09	0.012

Fig. 3.5, 3.6, 3.7 present the heave, pitch and roll RAOs of fish farm body in three wave directions. Owing to the symmetry of farm structure, wave direction shows little influence on the response of heave motion. However, roll and pitch motion present to have some difference.

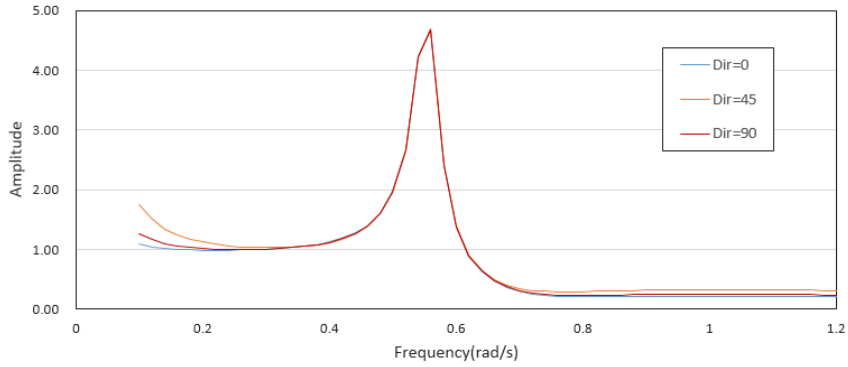

Figure 3.5: Heave RAOs with different wave directions

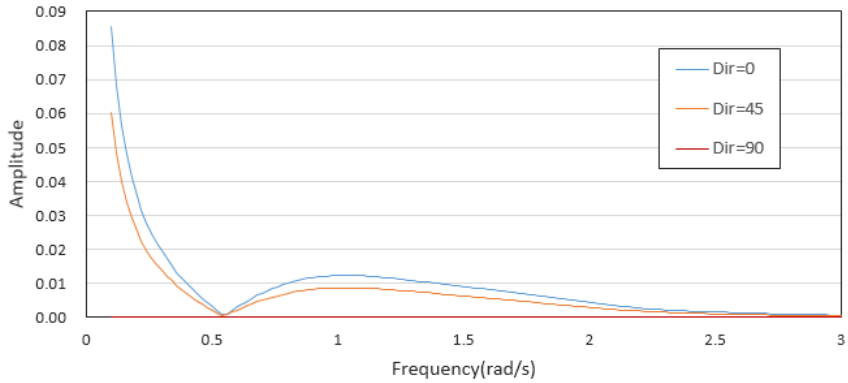

Figure 3.6: Pitch RAOs with different wave directions

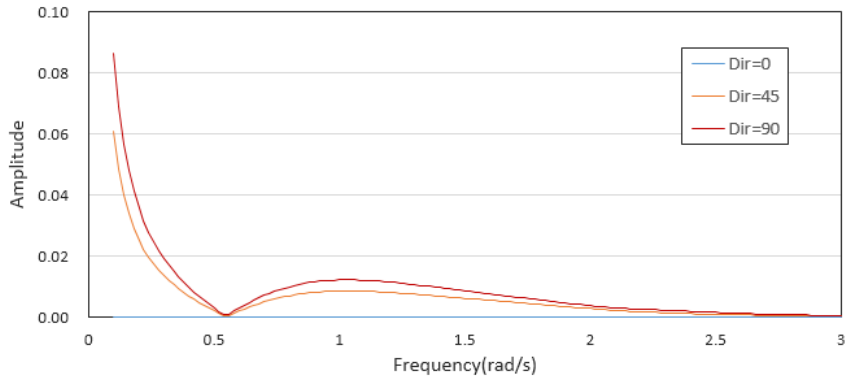

Figure 3.7: Roll RAOs with different wave directions

3.2 WASIM Analysis in Time Domain

WASIM is a program in HydroD software, using Morison equation and solving 3D diffraction/radiation problem by Rankine panel method (HYDROD, 2006). In this time domain simulation, the model of farm main body and location is set to be the same with the one in frequency domain. What makes the difference is that six anchor elements are deployed at the bottom of net frame cylinders to keep position. Wave following PM spectrum is applied in the environment condition, where significant wave height $Hs = 4m$ and wave period $T = 10s$. Current is not included in this case.

HydroD provides anchor elements available for connecting with Morison model. The fair leads and configuration of the anchor elements are illustrated as Fig. 3.2. The anchor elements are simplified from mooring system with only linear stiffness characteristics. Therefore, the analysis is quasi-static coupled in this simulation. During the calculation process, the mooring forces on farm body would be calculated as the following procedure:

1. The fairleads on farm body deliver its displacement to anchor elements.

2. The restoring force of anchor elements is calculated.

3. The force of mooring system is transformed back to farm structure.

The data of the anchor elements are listed as the following Tab. 3.3, where the horizontal and vertical stiffness is specified according to the data from SIMA mooring analysis.

Table 3.3: Parameters of anchor element

Angle with horizontal plane	Horizontal stiffness	Vertical stiffness	Pre-tension
40 deg	90 kN/m	30 kN/m	120 kN/m

3.2.1 Convergence Study of Mesh

A study is carried out under the same environment condition to check the convergence of the model mesh. The simulation time is set to be 200s. Fig. 3.8 shows the comparison of different model mesh. From model 1 to 2 and model 2 to 3, the water surface mesh as well as model panels are increased 200% and 150% respectively. Since model mesh in model 2 and 3 are denser than model 1, the computation time is much longer. This study aims to check whether model mesh 1 is accurate enough and the necessity of increasing mesh density.

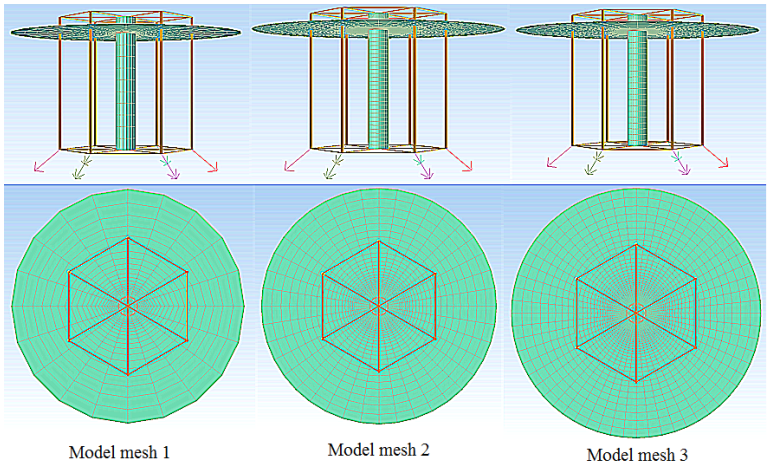

Figure 3.8: Comparison of model mesh in convergence study

The results of the convergence study on surge and pitch motions are shown as Fig. 3.9 and 3.10 (Initial mesh, modified mesh and final mesh represents model mesh 1, 2 and 3 respectively). Due to space limitation, the other motions' convergence study results are listed in appendix A. The graphs indicate that the peak of initial mesh is higher than the one in final mesh, while the modified mesh is almost coinciding with the path of final model. Therefore, it can be concluded that model mesh 1 is too coarse for simulation and not accurate enough. On the other hand, model mesh 2 shows sufficient accuracy with relatively low mesh density and computation time, meaning model mesh 2 would be the most suitable one in the later time domain simulation.

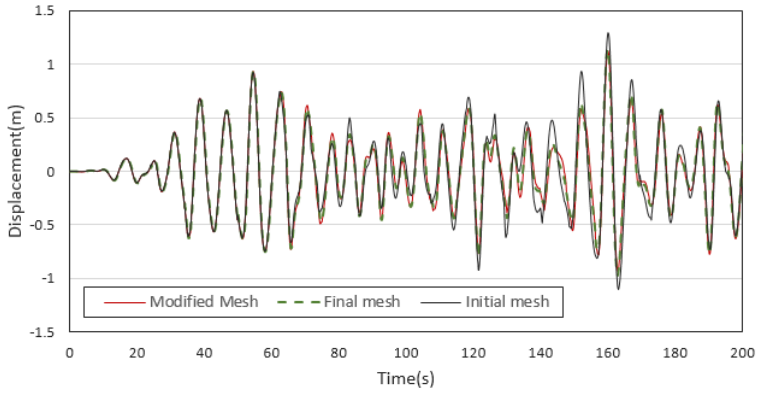

Figure 3.9: Convergence study of surge motion

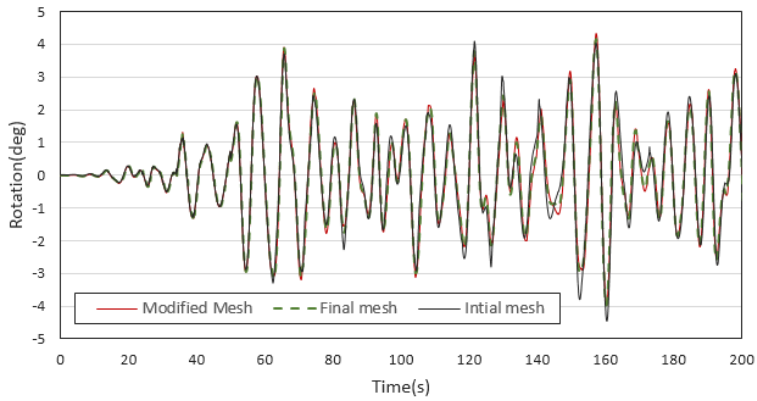

Figure 3.10: Convergence study of pitch motion

3.2.2 Comparison of Time Domain and Frequency Domain Results

In this comparison, both of the simulations are carried out with a same quasi-static coupled model as illustrated above. For time domain simulation, the time increment is set as 0.1s, and a total length of 1000s simulation is implemented. For Frequncy domain simulation, the frequency set is the same as the previous one in WADAM analysis.

The simulations are carried out with incoming wave characterized by PM spectrum with significant wave height $Hs = 4m$ and peak period $T = 10s$. Current is not taken into consideration in this analysis. For the hydrodynamic loads in present simulations, the first order wave forces, added mass and radiation damping, the second order mean forces are applied. In frequency domain, nonlinear forces must be treated with stochastic linearization, while in time domain, the nonlinear forces are applied to farm body directly at each time steps (Ran et al., 1999). The results of time domain simulation are transferred through FFT function in MATLAB.

The comparison of surge, heave and pitch response spectrum are presented as following Fig. 3.11, 3.12, 3.13. It is observed that the response motions from time domain and frequency domain are generally similar. There is significant response in heave motion when we locate at the low frequency part. But the results of low frequency part are absence in frequency domain analysis, and thus it is hard to figure out the response difference at this location.

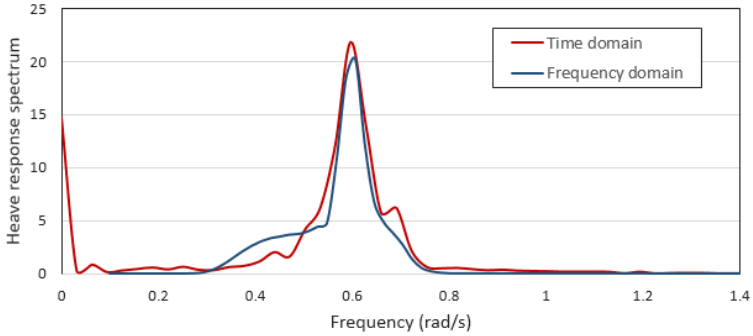

Figure 3.11: Response spectrum of heave motion

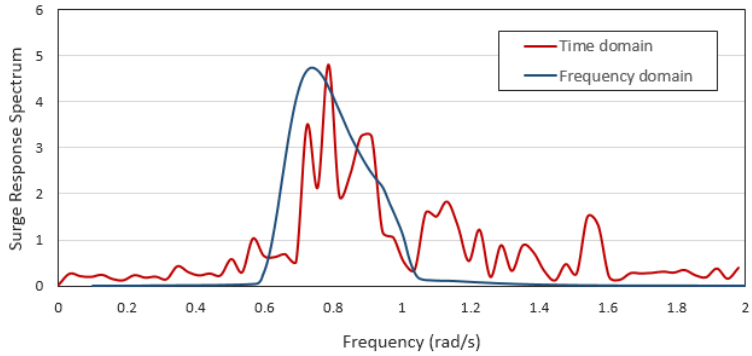

Figure 3.12: Response spectrum of surge motion

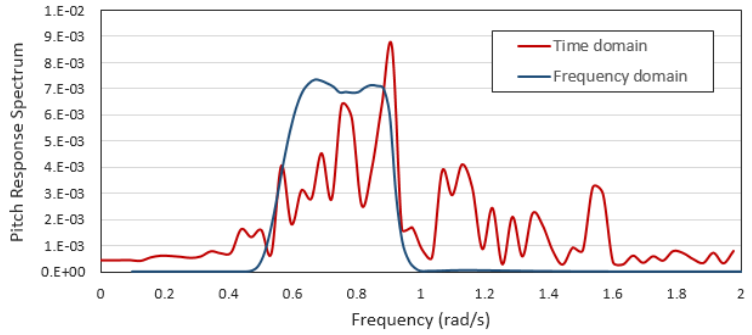

Figure 3.13: Response spectrum of pitch motion

For all of these three response spectra, the results from time domain seem to give slightly larger amplitude than frequency domain. According to the study of Ran, the reason could

be that the viscous damping in frequency domain is overestimated owing to stochastic linearization (Ran et al., 1999).

When we focus on the location of high frequency part, the surge and pitch motion response in time domain shows to be much larger than in frequency domain. This might also come from the limiting effect of viscous damping on high frequency motion.

Overall, the accuracy of frequency domain analysis is acceptable comparing with the results from time domain simulation. Considering much less computation load required in frequency domain analysis, it is still a useful approach for fast and approximate analysing of hydrodynamic properties.

Chapter 4

Dynamic Analysis of Coupled Model in SIMO

The dynamic response analysis can be carried out with both frequency domain and time domain method. In frequency domain, structure motion is described by a function of frequency. Whereas frequency is in a wide range, frequency domain would normally be suitable to test the hydrodynamic performance of the offshore structure. Moreover, there would be a less computational expense in frequency domain compared with time domain. However, Morison equation calculated in frequency domain is linearised with stochastic approach, which might contribute to overestimation of viscous damping and other nonlinear effects (Zhang et al., 2008; Ran et al., 1999). In this situation, the accuracy of the analysis might not reach the desired level.

For analysis in time domain, the motion of offshore structure is observed as a function of time. Nonlinear loads are applied instantaneously on the farm body and mooring lines, leading to higher accuracy. Furthermore, developing phenomena in the real condition is capable for study. Therefore, time domain is preferred in analysing the motion in specific sea states. In this chapter, time domain analysis will be implemented to simulate the response of coupled model (Li et al., 2018).

The simulation is carried out in SIMO program, which provides a coupling model of rigid body and catenary system. For fish nets, the model is simplified to be slender rigid beams based on sensitivity study. The results of the simulation aim to check the response of fish farm structure under different sea states and compare the performance of mooring system with various mooring line pre-tensions. In addition, with time domain results of simplified mooring model from WASIM, a comparison will be carried out to figure out the difference between coupled system and quasi-static coupled one.

4.1 Simulation Program

SIMO is a time domain simulation program in SIMA workbench developed by Sintef. Non-linear analysis is available in SIMO for simulating oscillating and station keeping process of multibody systems. The program uses the convolution integral approach to solve the formulation. And Simulation results obtained from SIMO are presented as time traces, spectral analysis and statistics of all motions and forces of all bodies in the analysed system (Reinholdtsen and Falkenberg, 2001).

The program is divided into 5 separate modules communicating through a file system as illustrated in Fig. 4.1.

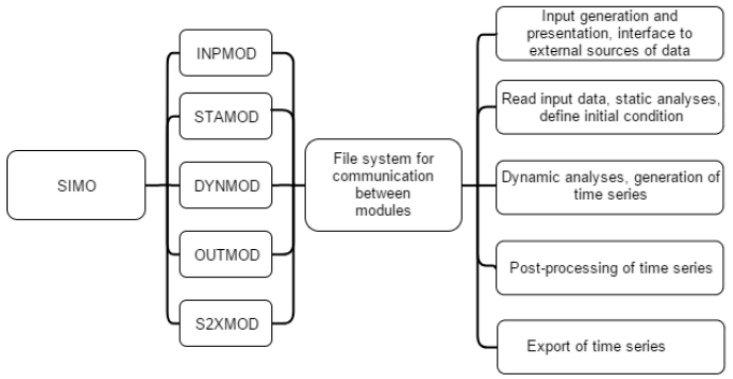

Figure 4.1: Modules of SIMO program (Reinholdtsen and Falkenberg, 2001)

4.2 Modelling of Mooring System in SIMO

The positioning system is of great importance for offshore structure to withstand loads from wave, currents and wind, and keep position in various sea states. There are normally two kinds of positioning system for offshore structure, dynamic positioning system and mooring system. The first one makes use of thrusters to create opposite force with hydrodynamic loads and maintain stationary. Since it generally costs a lot to install thrusters, dynamic positioning system would be suitable for offshore structure with huge dimension other than offshore fish farm. In this thesis, mooring system will be applied on offshore fish farm to keep position (Faltinsen, 1993).

In this section, a mooring system with six mooring lines is set up in SIMO program to provide positioning forces. Mooring lines are assumed to be in form of catenaries, where catenary equations would be used to model them. The program constructs the catenary mooring lines based on methods in mooring analysis program MIMOSA. While MIMOSA operates mooring lines in frequency domain with linearization operation, SIMO extends to time domain and treats them as individual elements. It is capable for the program to execute either quasi-static analysis or simplified dynamic analysis, which accounts for the drag effect on mooring lines. (Marintek, 2017).

To get a more accurate result of mooring line behaviour, simplified dynamic analysis is carried out in the thesis, in which the effect of transverse drag loads on mooring lines is taken into account. Due to dynamic effect of hydrodynamic force, the line tension may deviate from the tension provided by quasistatic analysis (Marintek, 2017). The total line tension is thereby calculated from two parts: one is velocity and acceleration induced by the hydrodynamic loads, and the other would be determined by the relative location of top end and anchor. Out of this situation, a dynamic tension computation model developed by Larsen and Sandvik is applied for simulation as illustrated in theory chapter (Larsen, 1990).

4.2.1 Static Calculation

To analyse the mooring system, a static calculation is usually conducted at the initial design stage. During the process, load characteristics and configuration of mooring lines are defined for later dynamic calculation.

For static calculation in SIMO, the mooring line configuration can either be specified by line pretension or anchor position when the total length of the mooring line is determined. In this thesis, the mooring system is defined by pre-tension at the fairlead of mooring lines. And the following equations are used in MATLAB (detailed scripts in Appendix B) to calculate the position of points with a length of 1m (Høiland, 2017).

$$F_h = T_{pre} * \sin(\phi) \tag{4.1}$$

$$S_x = \frac{F_h}{w} \cosh^{-1}\left(\frac{w * d}{F_h} + 1\right) \tag{4.2}$$

$$S_y = \frac{F_h}{w} \cosh\left(\frac{w * S_x}{F_h} - 1\right) \tag{4.3}$$

$$S = \frac{F_h}{w} \sinh\left(\frac{w * S_x}{F_h}\right) \tag{4.4}$$

$$T = \sqrt{F_h^2 + (w * S)^2} \tag{4.5}$$

Where d is the water depth of mooring line elements, S_x and S_y is the horizontal and vertical distance from top end to touchdown point respectively, T_{pre} is the pretension of mooring lines, ϕ is the pre-angle between lines and vertical, S is the length of catenary line, T is the total tension, F_h is the horizontal tension, w is the mooring line weight per unit length in water.

With the equations provided above, the results listed in Tab. 4.2 are calculated from input mooring line characteristics in Tab. 4.1. The configuration of the mooring line is shown in Fig. 4.19 (Blue line).

Table 4.1: Input characteristics for mooring lines

Characteristics	Units	Value
Water depth	m	100
Submerged weight	Kg/m	71
Pretension	kN	120
Preangle	deg	35
Total length of catenary line	m	250

Table 4.2: Calculation results from MTALAB

Characteristics	Units	Value
Horizontal tension on top end	kN	68
Horizontal length of catenary line	m	130
Total length	m	172
Distance from touchdown point to anchor	m	78

4.2.2 Mooring Lines Setup

According to the static calculation results of mooring line characteristics, the configuration of the mooring system with pretension 120 kN is plotted as following Fig. 4.2. The fairleads of mooring lines are installed at the bottom of each vertical cylinder. Such a configuration will be beneficial for the structure to achieve minimal rolling and pitching motion. The angle θ between two mooring lines is defined as 60deg as illustrated in Fig. 4.3.

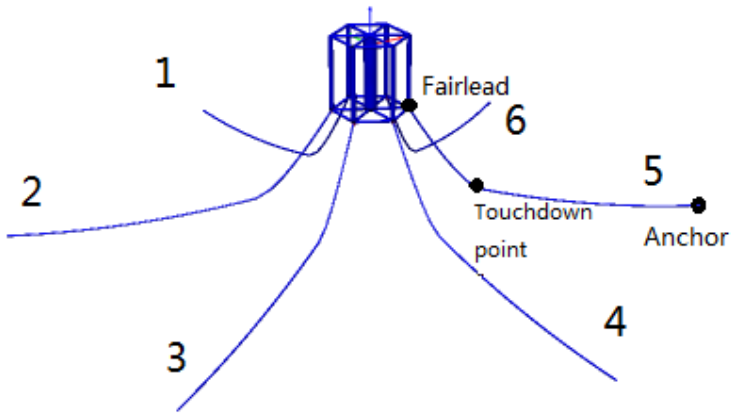

Figure 4.2: Mooring system configuration with lines number

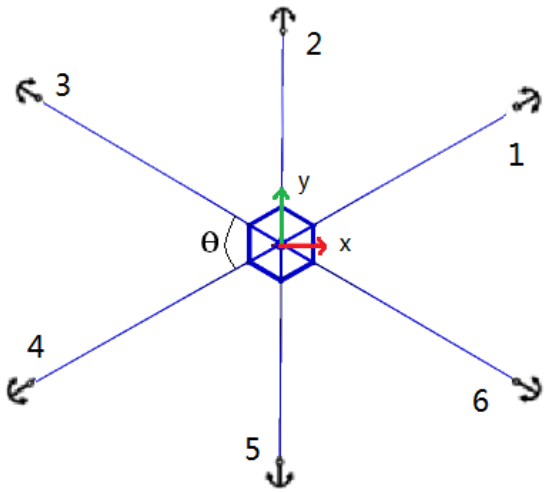

Figure 4.3: Mooring system configuraion from topside

Tab 4.3 lists the parameters of mooring lines for dynamic simulation. Steel linked chain segments are selected to provide adequate restoring forces for the mooring system. For simplification, The wire rope is not used here, and the link segment is also neglected. Notably, there should not be a vertical force on an anchor, which may lead to failure of the mooring system. To avoid the collapse, a length of 250m chain is chosen to leave enough distance between touchdown point and anchor.

Table 4.3: Mooring line parameters

Characteristics	Units	Value
Total length	m	250
Diameter	m	0.09
Elasticity modulus	N/m^2	5.0e10
Segment type	-	Chain
Weight in air per unit length	Kg/m	79.2
Bottom friction	-	1
Transverse drag coefficient	-	2
Longitudinal drag coefficient	-	0.4

4.3 Modelling of Fish Nets

Generally speaking, two approaches are available while modelling the fish nets for hydrodynamic loads calculation. One is to calculate the loads on each knot and twine of the nets. The total force is then figured out by the sum of loads on these individual elements (Lader et al., 2003). It is a high accuracy method giving detailed loads and response of each net elements, though a large number of computational resources are required.

The other approach is to model the net as several super elements instead, which can simulate the behaviour of a set of net knots and twines. The force acting on the nets are calculated by means of drag and lift coefficient, which depends on the solidity ratio Sn of nets (Løland, 1991). Fewer elements result in reduced accuracy, while the computation time also gets a significant reduction. For fish nets with small deformation, calculating hydrodynamic force with super elements shows to be an effective method that provides reliable results. And this is the reason why the method is chosen to simulate net panels in this thesis.

As mentioned before, the fish nets of offshore fish farm model are restricted in the frame of the steel structure. The deformation of fish nets is quite limited according to the simulation results of the truss model, where the largest deformation is less than 1.5m for EC1 in Tab. 4.4.

Table 4.4: Environment condition of regular wave and constant current

EC No.	Amp (m)	T (s)	V_c (m/s)	Dir_w (deg)	Dir_c (deg)
EC1	2	4	0.5	0	0

As the deformation is negligible, fish nets in SIMO simulation could be simplified as rigid slender elements. Moreover, the number of beam elements are reduced for faster

calculation. In order to check the reliability of simplification, a sensitivity study is thus implemented to test the simplified model.

4.3.1 Sensitivity Study of Rigid Beam Nets

The test modeled two different fish nets, one is Truss model using rope material with diameter $Dt = 0.065m$, gap $Lt = 1m$ and the other is rigid beam model with diameter $Dr = 0.065m$, gap $Lr = 5m$, as shown in Fig. 4.4. Each corner of the frame (regarded as a rigid body) is fixed in x, y and z-direction, namely $dx = dy = dz = 0$. The environment condition is applied according to EC1 in Tab. 4.4.

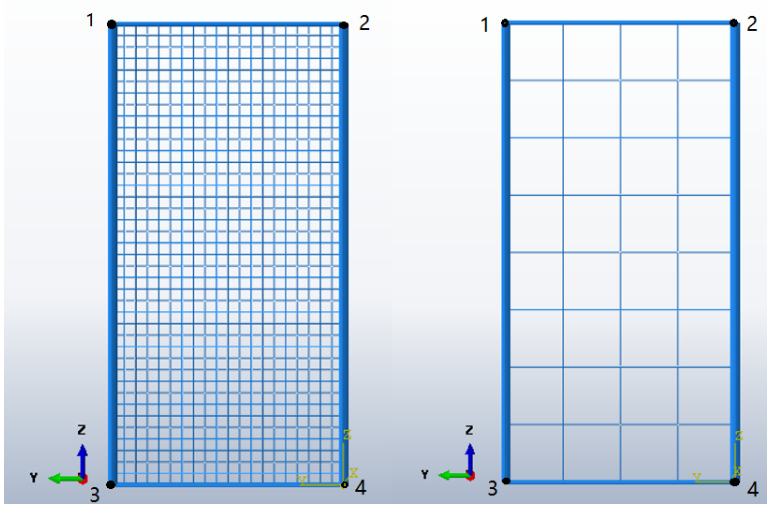

Figure 4.4: Truss model (left) and rigid beam model (right)

With slender beam elements, Morison equation is applied to calculate the mean hydrodynamic loads on the panel per unit length:

$$F = \frac{1}{2}\rho C_d^{\text{beam}} D^{\text{beam}} \cdot (V_c + V_f - \dot{a})|V_c + V_f - \dot{a}| + \rho C_m^{\text{beam}} \frac{\pi}{4} \left(D^{\text{beam}}\right)^2 \cdot \ddot{a} \quad (4.6)$$

Where $\dot{a}$ and $\ddot{a}$ are the model velocity and acceleration respectively, V_c is the current velocity, V_f is the fluid particle velocity, ρ is the water density, D^{beam} is the equivalent outer diameter of Morison beams, C_d^{beam} is the equivalent drag coefficient, C_m^{beam} is the equivalent mass coefficient.

To achieve the equivalent solidity ratio with real nets, the equivalent drag coefficients are calculated according to the diameter of the beam by Eq. (4.7). This formula can also

act on lift coefficient. Furthermore, as discussed in hydrodynamic loads section, the mass coefficient of net twines C_m^{twine} is set to be 2. And thus, the equivalent mass coefficient for beam and truss can be computed with Eq. (4.8).

$$C_d^{\text{beam}} \cdot D^{\text{beam}} = C_d^{\text{panel}} \cdot A^{\text{panel}} \tag{4.7}$$

$$C_m^{\text{beam}} \cdot \left(D^{\text{beam}}\right)^2 = n \cdot C_m^{\text{twine}} \cdot \left(D^{\text{twine}}\right)^2 \tag{4.8}$$

Where n is the amount of net twines replaced by rigid beams, panel drag coefficient C_d^{panel} of net panel are defined according to Eq. (2.36) (2.37) as discussed above.

The results of the reaction force on node 2 and 4 in Fig. 4.4 are recorded in time domain simulation. Since the direction of incoming wave and currents are 0deg, nodal force in x-direction are concerned. Fig. 4.5 shows that on node 2, force calculated from beam model is about 10% larger than the result from truss model, which means the loads were overestimated in the rigid beam model. And on node 4, beam model gets a very similar result with truss model as shown in Fig. 4.6.

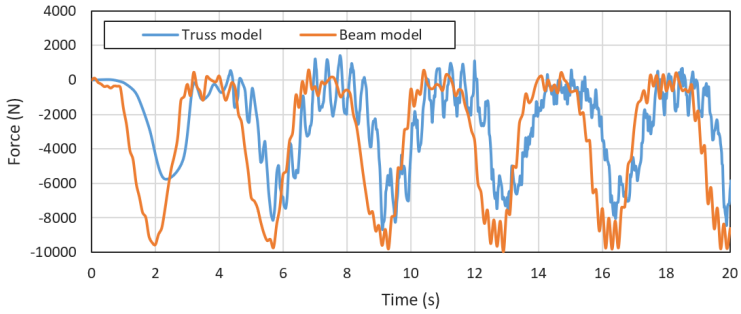

Figure 4.5: Nodal force in x direction at node 2 from beam model and truss model

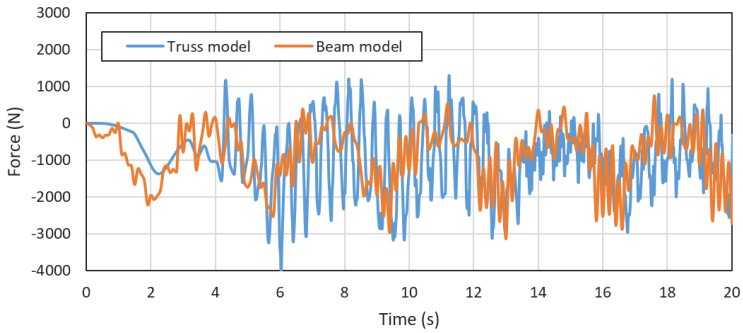

Figure 4.6: Nodal force in x direction at node 4 from beam model and truss model

4.3.2 Fish Nets Setup

According to the graphs, it is evident that beam model will result in overestimating of force compared with truss model, but the deviation of force is still acceptable for dynamic analysis of farm structure. Therefore, the rigid beam model will be used in this thesis to calculate the hydrodynamic loads from fish net panels.

In SIMO program, the fish nets are modeled by slender elements with the same geometry as the beam model in ABAQUS. Tab. 4.5 lists the specific parameters of beam elements. Moreover, there are current velocity reduction phenomena, which causes a reduction of velocity when the current flow through the latter net panels. However, since the nets are modeled as rigid bodies, the velocity reduction factor is not able to be calculated in SIMO program. To fix the problem, the drag coefficient of latter net beams are decreased instead to reduce the total hydrodynamic force (Lader and Fredheim, 2006).

Table 4.5: Data of net beams in SIMO

Parameters	**Symbol**	**Units**	**Value**
Net mass	M	kg/m	18.56
External area	S_{ex}	m^2	0.0033
Cross-section type	-	-	Rigid beam
Tangential drag coefficient	C_{dt}	-	0.05
Normal drag coefficient	C_{dn}	-	6.75
Added mass	A_m	kg/m	2.0

4.4 Environment Condition

A sea state is normally specified by the following parameters: wave spectrum with significant wave height, mean wave period, mean propagation direction and spreading function. In engineering application, the first two parameters are the most important characteristics, and the sea state is assumed to keep a stationary random process during a period. The period of the stationary is taken to be 3 hours in this thesis, the same as standard value, while it can actually vary from 0.5 to 10 hours (DNVGL, 2017)

Wave is a result of wind activity but also influenced by interaction among waves. Therefore, wave conditions are usually separated into two categories: wind sea and swell. Swells are generally travelled from the area far from the location. Wind sea represents waves caused by local wind. In this thesis, the wind seas will be the focus of discussion. Tab. 4.6 presents the Douglas Sea state scale adopted by the World Meteorological Organization (WMO), which measures the height of the waves and also the swell of sea (Zheng et al.,

2018).

Table 4.6: Douglas Sea state scale of wind sea (Zheng et al., 2018)

Sea states	Significant wave height (Hs)	Wind velocity (v)	Description
0	0.0 m	-	Calm (glassy)
1	0.0-0.1 m	-	Calm (rippled)
2	0.1-0.5 m	<3.6 m/s	Smooth
3	0.5-1.25 m	3.6-6.2 m/s	Slight
4	1.25-2.5 m	6.2-8.2 m/s	Moderate
5	2.5-4.0 m	8.2-10.0 m/s	Rough
6	4.0-6.0 m	10.0-12.0 m/s	Very rough
7	6.0-9.0 m	12.0-15.5 m/s	High
8	9.0-14.0 m	15.5-23.2 m/s	Very high
9	> 14.0 m	> 23.2 m/s	Penomenal

Whereas the offshore fish farm is designed to be operated in the East China Sea, the environment condition (EC) is considered to refer to the sea states of Chinese ocean. In this thesis, the environment conditions are generated according to the statistics published by Zheng Kaiwen. In addition, the models of wave and current are built up based on standard DNV-RP-C205, which gives a detailed explanation of environment condition modelling as introduced in the theory chapter (DNVGL, 2017)

In Zheng Kaiwen's study, "significant wave height and wind speed data were analysed at a 6-hour duration for 30 years in the East China Sea". Fig. 4.7 illustrates the statistics of significant wave height probability distribution for various sea states in the East China Sea. On the other hand, Fig. 4.8 gives out the distribution of wind speed data. The white box in the graph is the target area for the offshore fish farm. The information is in form of cumulative frequencies f(Hs), which is a percentage calculated from (Zheng et al., 2018):

$$f(Hs) = \frac{n_h}{N_h} \tag{4.9}$$

where n_h is the number of Hs satisfies the defined range, N_h is the amount of Hs values. And the cumulative frequencies f(v) is presented as:

$$f(v) = \frac{n_v}{N_v} \tag{4.10}$$

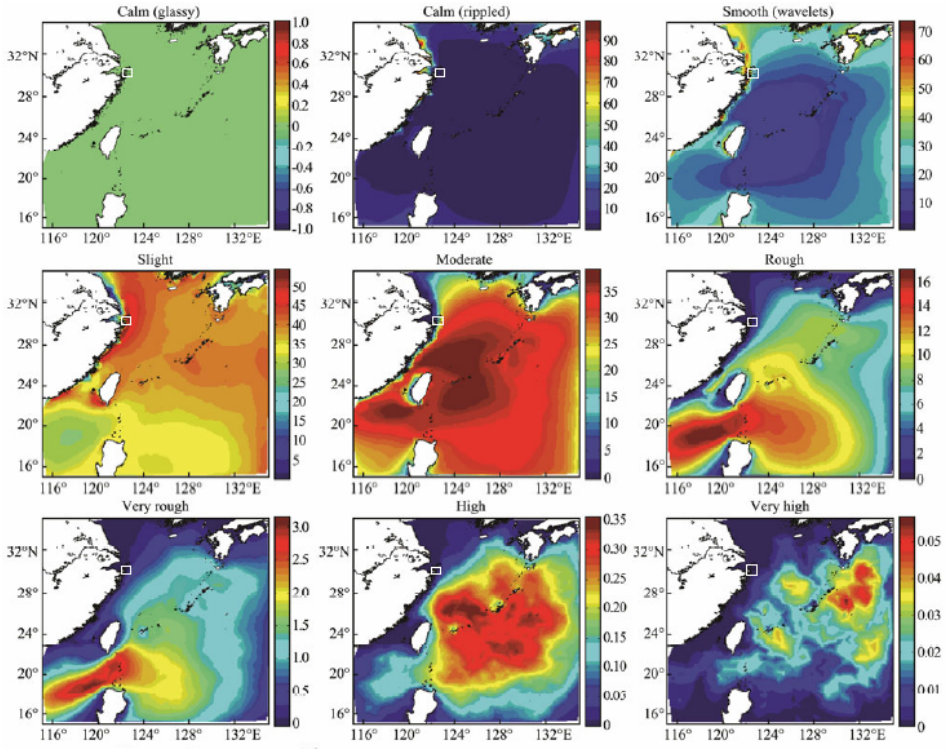

Figure 4.7: Statistics of significant wave height (Hs) probability distribution for various sea states in the East China sea (Zheng et al., 2018)

4.4.1 Modelling of Wave and Current

Generally, dynamic response analysis under a wide range of wind, wave and currents conditions is required at the design stage of offshore structures. And both operational and ultimate states should be considered to show the feasibility of structures. However, due to the limitation of fish farm operational regulation and reference, only ultimate sea states are concerned. In addition, with limited volume above the water surface, the wind effect of farm structure is neglected.

According to the Douglas Sea state scale and statistics of the East China sea provided in Fig. 4.7 and 4.8, it can be observed that the probability of rough and very rough sea state in the target area is about 1% and 0.1% respectively. The frequency of very high and phenomenal sea states is even smaller and negligible. And thus, the simulation in this thesis is going to take $Hs = 4m$ as ultimate ocean condition.

The research published by Zhu Yanrong shows the applicability of various wave spectra on Chinese ocean. Pierson-Moskowitz (PM) spectrum shows to be similar to the actual state of wave spectra (Zhu Yanrong, 1995). Therefore, the irregular waves in the simulation are

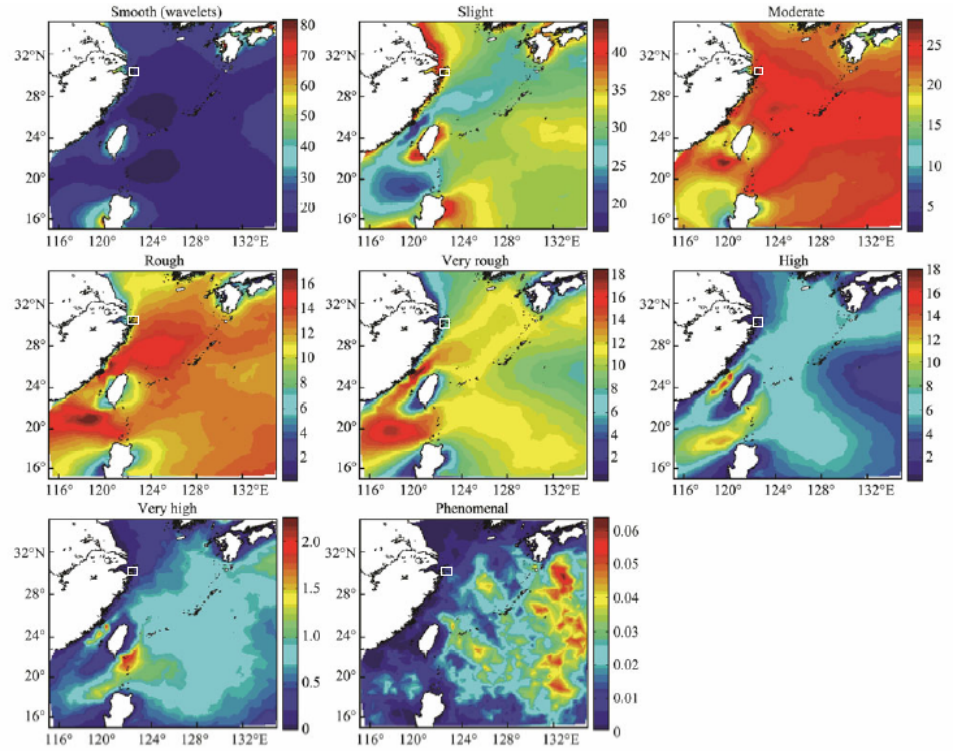

Figure 4.8: Statistics of wind velocity (v) probability distribution for various sea states in the East China sea (Zheng et al., 2018)

described by PM spectrum depending on significant wave height (Hs) and peak period (T), which is in form of:

$$S_{PM}(\omega) = \frac{5}{16} \cdot H_S^2 \omega_p^4 \cdot \omega^{-5} \exp\left(-\frac{5}{4}\left(\frac{\omega}{\omega_p}\right)^{-4}\right) \tag{4.11}$$

Where $\omega_p = 2\pi/T$ is the angular spectral peak frequency.

A total of seven environment conditions (EC) are involved in the simulation as shown in Tab 4.7. Fig. 4.9 gives out the configuration of the wave transfer direction. EC2 and EC3 exclude the effect of current, representing slight and moderate wave conditions in the East China Sea. Apart from wave, current is also an important factor in dynamic response. Two kinds of current velocity ($V_c = 0.25m/s$) and ($V_c = 0.5m/s$) are applied in EC5 and EC6 respectively to observe the current effect. Whereas the offshore fish farm has a large vertical dimension, the current speed in different depth may vary from the sea surface. Thus, a linearly decreasing current is used in the simulation, where the current speed is decreased to zero at sea bed. In addition, a phenomenon that current and wave approach the structure

from different direction might happen in reality. The misalignment between current and wave will also influence the response motion of structure and the mooring line tension. A misalignment of 30 degree is therefore implemented in the largest wave condition to study the influence.

Table 4.7: Environment condition of irregular waves and currents

EC No.	**Hs (m)**	**T (s)**	**Vc (m/s)**	Dir_w **(deg)**	Dir_c **(deg)**
EC2	2	6	0	0	-
EC3	3	8	0	0	-
EC4	4	10	0	0	0
EC5	4	10	0.25	0	0
EC6	4	10	0.5	0	0
EC7	4	10	0.5	90	90
EC8	4	10	0.5	90	30

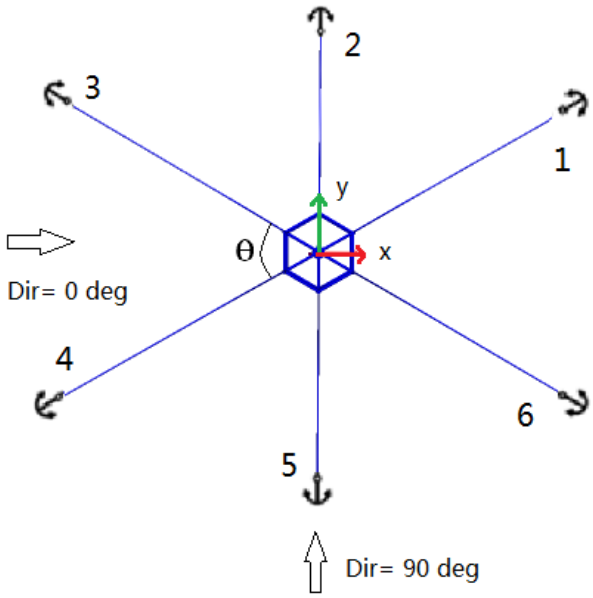

Figure 4.9: Configuration of wave and current direction

In the coupled time domain analysis, a 20 minutes simulation with a time increment of 0.01 s is carried out. But due to the limitation of calculation time, all of these environment conditions use 2 different seeds, and thus a limited variability of stochastic waves is taken

into account.

4.5 Kinetics of Farm Structure from Frequency Domain Analysis

In this thesis, the fish nets, as well as mooring system, are modeled as in SIMA program. However, for the kinetics of the farm main body, the characteristics are imported from results of frequency domain analysis in WADAM program (Høiland, 2017). The simulation is carried out the same as the one in the previous section. Tab. 4.8 lists the input parameters from WADAM analysis. The wave drift force is computed through the mean drift coefficient based on Newman approximation (Newman, 1974).

Table 4.8: Input parameters from WADAM analysis

Parameters	**Data**
Structure Model	Geometry, structural mass, center of gravity, moment of inertia
Damping	Linear damping matrix
Hydrostatic stiffness	Stiffness matrix
Wave force	First order wave force transfer function, wave drift force
Motion function	First order motion transfer function
Radiation data	Retardation function, frequency dependent added mass and damping

For all of the simulation conducted in this time domain analysis, the reference point for structure translation and rotation motion is located at the centre of the fish farm, coincide with water surface.

4.6 Results of Dynamic Analysis in Time Domain

In this section, the results of response motions and the mooring line tension will be compared in different environment condition provided above. The outputs of time domain simulation present the dynamic performance of farm structure from the initial static state to its equilibrium stage in various environment conditions.

For all of the simulations carried out in this thesis, the mooring line shows to be capable of withstanding the hydrodynamic loads from waves and currents. None of the simulations lifts the mooring lines from the seabed from the view of dynamic animation, which means the mooring line capacity is sufficient for the farm structure. Moreover, the tensions in

mooring lines were also kept at an acceptable level and did not exceed the maximum tension limit ($T_{max} = 1 * 10^6 N$) as shown in the Tab. 4.9. Due to the symmetry of mooring line distribution, only the tensions in mooring line 4, 5 and 6 are presented.

4.6.1 Mooring Line Tension

According to the data provided in Fig.4.10, it is obvious that when the incoming wave and current are in direction of 0 degree (namely EC2 to EC6), mooring line 4 will suffer the largest deformation and provide the main resisting force. However, for the direction of 90 degree (namely EC7), line 5 tends to have the largest tension among mooring lines, and even larger than the tension recorded in EC6. This mainly because the resisting force in EC6 is allocated to line 3 and 4, where both mooring lines are available for withstanding hydrodynamic loads. This indicates that incoming direction of 90 degree might be the most vulnerable situation for the farm structure.

Comparing the condition EC2 to EC6, while the mooring lines of no current ECs have a limited tension, currents in EC5 and EC6 increase the maximum tension significantly. The tension increased by 15% when a current velocity of 0.25 m/s is applied. For the variation of wave height, mooring lines tend to be less sensitive, but a slight rising of tension is still observed. The reason might be that the mooring tension is related to the drift motion of the structure, and the drift motion is mainly caused by wave drift force. Although the wave height increases for different ECs, the wave drift force appears to be steady in these cases.

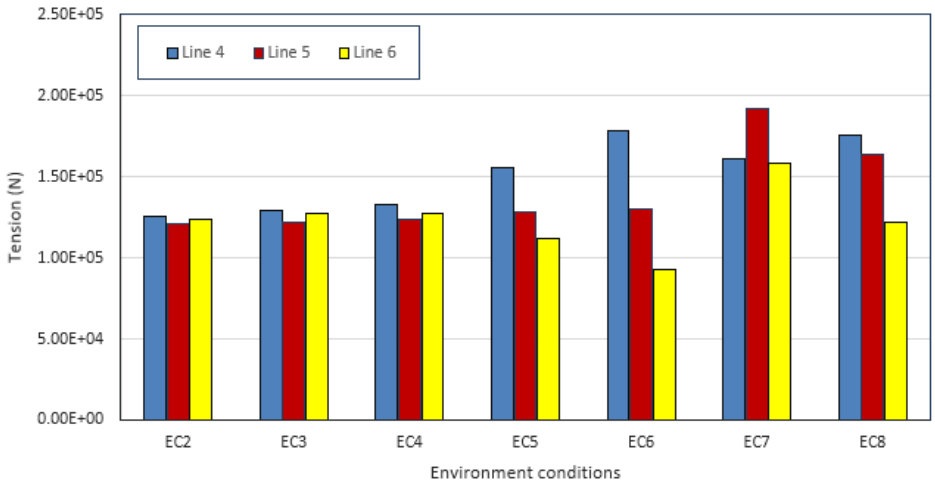

Figure 4.10: Comparison of maximum tension in different mooring lines

Tab. 4.9 compares the mooring tension data of dominating mooring lines in steady phase. The most severe condition appears in EC7, where the highest wave and the largest current

velocity with a direction of 90 degree are applied. The maximum tension of mooring line reaches 192 kN, 8% larger than the one in EC6. And the deviation of tension also shows to be more severe.

Table 4.9: Mooring tension data for the dominating mooring line

EC No.	Line No.	Maximum tension (kN)	Mean tension (kN)	Standard deviation (kN)
EC2	4	125	122	1.61
EC3	4	129	122	3.55
EC4	4	132	124	3.79
EC5	4	156	144	5.18
EC6	4	178	167	5.35
EC7	5	192	172	6.54
EC8	4	176	166	4.10

For the performance of mooring lines in EC8, the misalignment of wave and current disturbs the symmetric distribution of force in mooring lines. Fig. 4.11 presents the historical tension in different mooring lines under the condition of EC8. Line 3, 4 and 5 appear to suffer larger tension than the rest of lines. Comparing to EC6, the mean mooring tension of these lines is quite similar. Furthermore, the largest deformation arises in line 4, meaning that the current force dominates the tension of mooring lines rather than the second order wave drift force in this case.

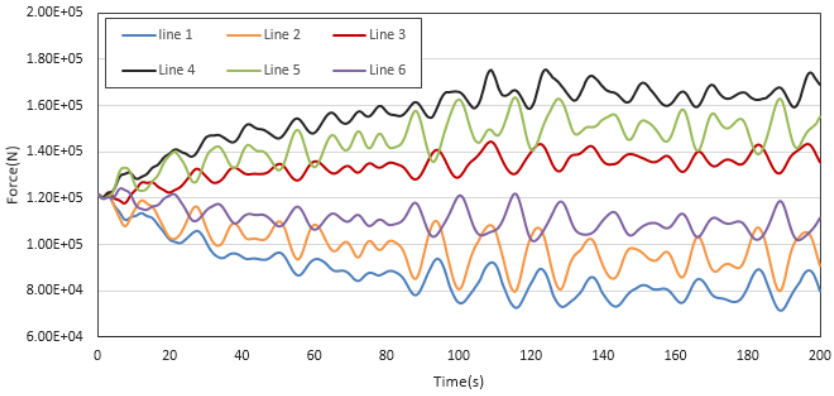

Figure 4.11: Mooring line tension in EC8

4.6.2 Response Motion

In the simulation of EC2 to EC6, the drift motion only occurs in the x-direction, because the incoming wave and current are both in direction of 0 degree. Similarly, drift off of EC7 only occurs in y-direction. However, in EC8, the wave and current approach the structure from different directions. And thus, the drift motion is calculated by the largest displacement in XY plane. Fig. 4.12 illustrates the drift off appeared in EC6, EC7 and EC8. The maximum drift off reaches about 16m in EC6, 33% larger than EC7 and 45% larger than EC8. It is evident that the wave and current direction of 0 degree show to have the most significant influence on mooring response. In contrast, direction of 90 deg implies a slighter motion response and smaller mooring tension. Therefore, the structure should encounter wave and current in direction of 0 deg when the farm structure is implemented in the real condition.

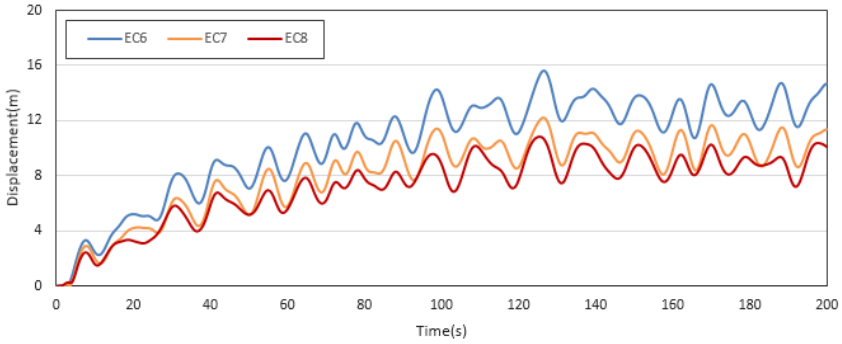

Figure 4.12: Drift motion in EC6, EC7 and EC8

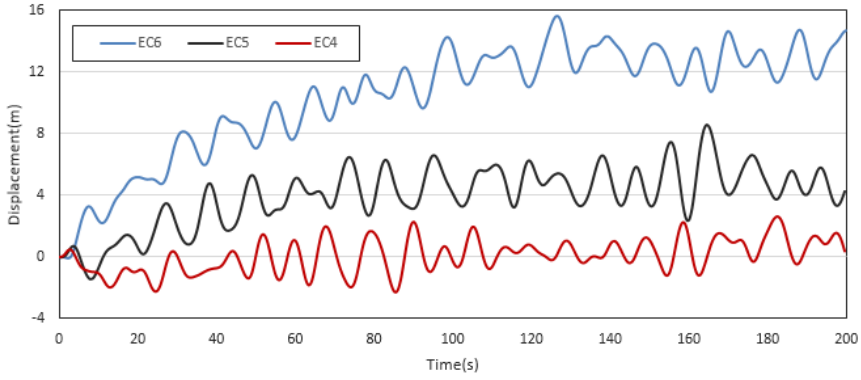

Figure 4.13: Drift motion in EC4, EC5 and EC6

Comparison of EC4, EC5 and EC6 in Fig. 4.13 verifies the influence of currents, where

different current velocities are applied in these three conditions. It is evident that the current causes most of the drift motion, while the wave drift force shows less influence. Whereas the maximum wave drift force in EC6 is 20 kN as shown in Fig. 4.14, the maximum hydrodynamic force reaches 600 kN, 30 times larger than the wave drift force.

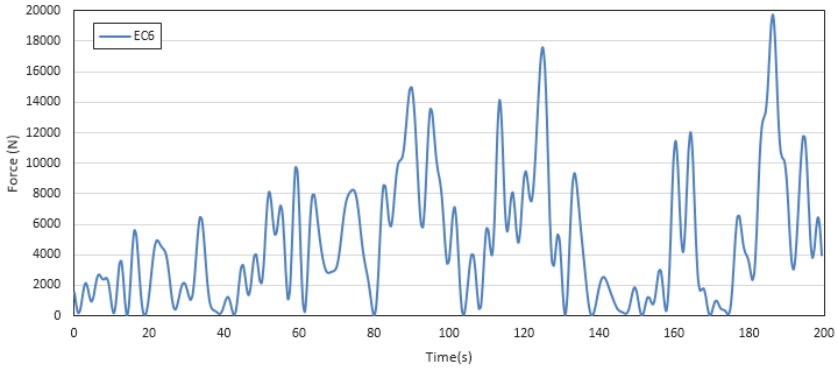

Figure 4.14: Wave drift force in EC6

For the sea states of no currents, drift motion comes to be less apparent, namely around 1m for EC4 and even less in EC2 and EC3. Fig. 4.15 presents the vibration of structure in x-direction. It is obvious that the response motion of the model tends to increase with the rising of wave height. The maximum displacement of EC4 is recorded as 3.1m, compared with 2m in EC3 and 0.8m in EC2.

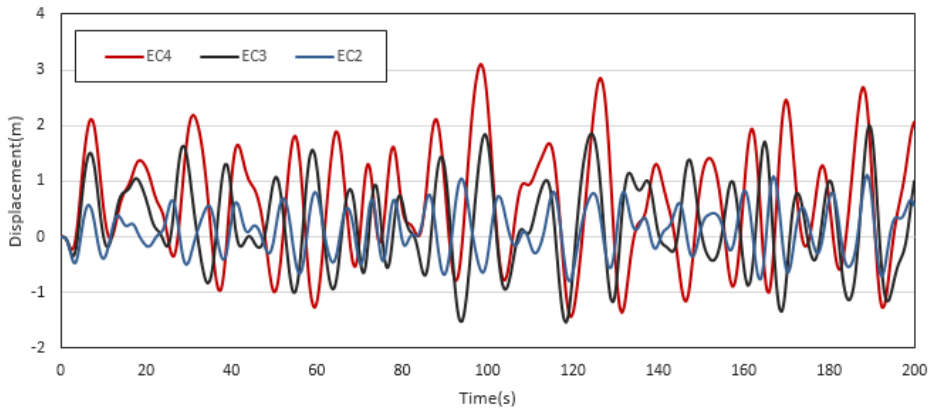

Figure 4.15: Drift motion in EC2, EC3 and EC4

Fig. 4.16, 4.17 and 4.18 give out the heave, roll and pitch motion of the farm model re-

spectively. Environment conditions of EC2, EC3, EC4 and EC6 are displayed in these graphs. For EC4 and EC6, the motion response shows to be quite similar to each other, which indicates that the currents have less influence on the motion of structure than the wave loads.

The heave motion for all of the cases is quite limited. The Amplitude of vibration is restricted in 0.15 m for EC4, 0.07 m for EC3 and 0.02 m for EC2. For the roll and pitch motion, wave loads appear to be rather significant. While the rotation of EC2 with a wave height of 2 m is less than 0.5 deg, wave height 4 m in EC4 leads to a rotation motion at around 8 deg. Therefore, there is a nonlinear relation between wave height and structure rotation motion.

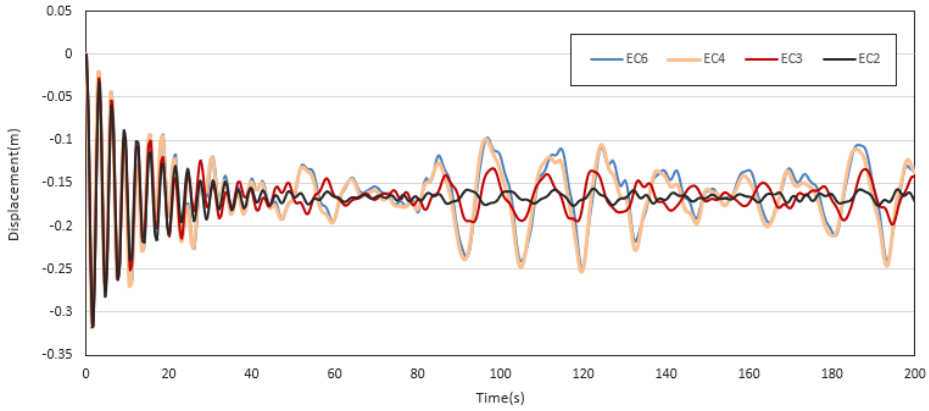

Figure 4.16: Heave motion in EC2, EC3, EC4 and EC6

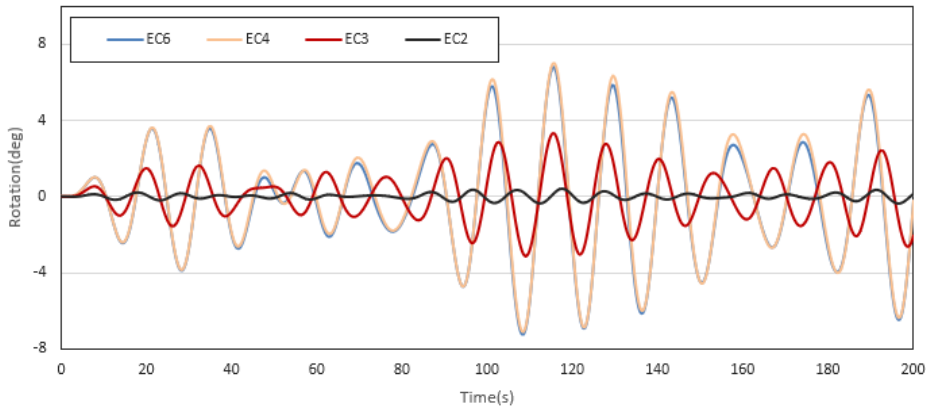

Figure 4.17: Roll motion in EC2, EC3, EC4 and EC6

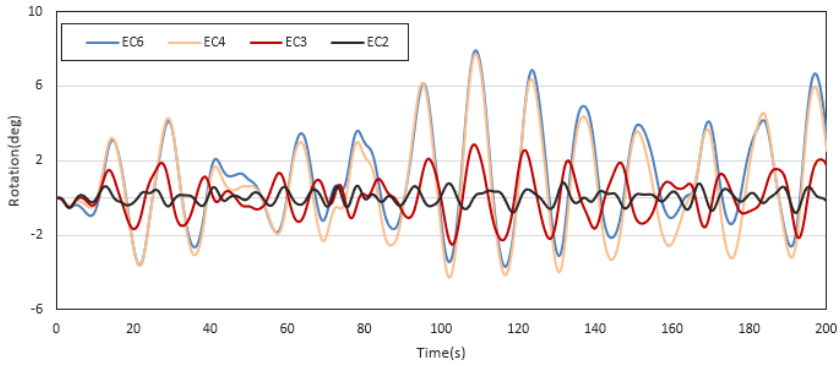

Figure 4.18: Pitch motion in EC2, EC3, EC4 and EC6

4.6.3 Comparison of Dynamic Response with Different Mooring Line Pre-tension

As illustrated in the theory chapter, the configuration of the mooring system is influenced by the pre-tension applied on the mooring lines. And therefore, different mooring line pre-tension will result in various dynamic response of farm structure. In this section, the effect of pre-tension will be studied. Three mooring line pre-tensions are applied, while all the other variables are set as constants, such as fairlead position, length, diameter, weight, etc.

The study is carried out in SIMA program with a simplified dynamic analysis of mooring system. The environment condition is selected as EC6, where both Current $V_c = 0.5m/s$, and wave $Hs = 4m, T = 10s$ exit. As the model of pre-tension $T_{pre2} = 120kN$ is already simulated, the farm structure is modeled the same as this simulation. Pre-tension in other simulation are chosen to be $T_{pre1} = 80kN$ and $T_{pre3} = 150kN$. Fig. 4.19 shows the configuration of mooring lines with various pre-tension.

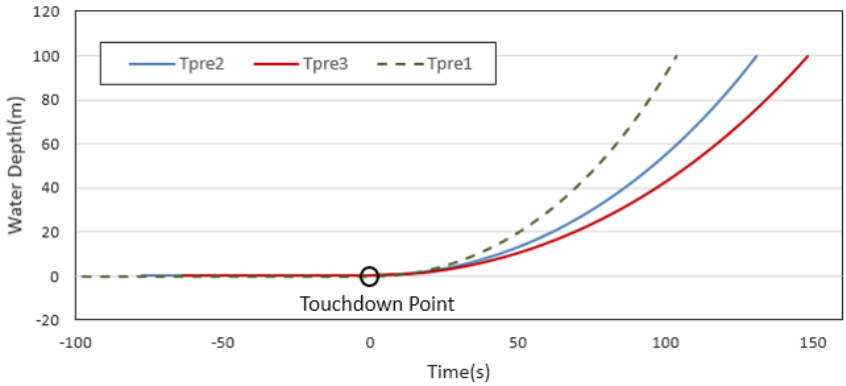

Figure 4.19: Configuration of mooring lines with various pre-tension

The results of drift motion are presented as Fig. 4.20. Whereas the response motions of heave, surge, pitch and roll are closely coincident, the graphs are listed in appendix C. It is evident that the mooring line pre-tension has limited effect on the oscillation motion of farm structure. However, when comparing the motion of drift, the result comes to be different. For mooring line pre-tension 1 and 2, it is observed that the curve has similar tendency, but the maximum drift of pre-tension 1 is slightly larger. In comparison, pre-tension 3 leads to a significant decrease in drift motion, nearly half of the displacement in T_{pre3}.

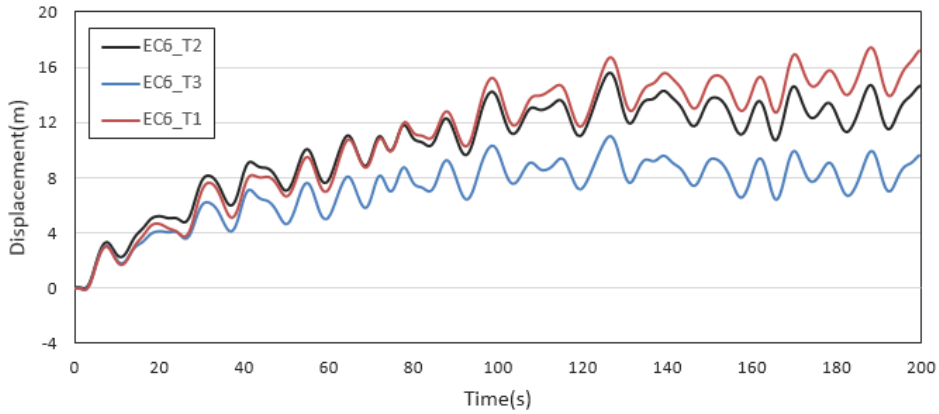

Figure 4.20: Comparison of fish farm drift with different mooring line pre-tension

This indicates that the mooring line pre-tension has a non-linear effect on the drift of floating farm body. The performance of the mooring system can be enhanced by increasing of mooring line pre-tension. But it will also contribute to the rise of mean tension on mooring lines, which means a stronger line must be used to prove the strength. In reality, there should be a balance between the cost of the mooring system and desired positioning

performance.

4.7 Comparison of Mooring System in SIMO and WASIM

In order to figure out the effect of coupled mooring system, the results from WASIM and SIMO simulations are compared. In WASIM, a quasi-static coupled mooring system is modeled based on massless linear spring. But for SIMO modelling, the mooring system is set up with catenary mooring lines. The same location condition and environment loads are applied in the simulations, where water depth $D = 100m$, PM spectrum with significant wave height $Hs = 4m$, wave period $T = 10s$. In SIMO simulation, the kinetics of the structure are imported from WASIM frequency domain results to ensure the same states.

The results of these two simulations are illustrated as Fig. 4.21 and 4.22. Both surge and pitch motion show similar response between SIMO and WASIM. When comparing the results of surge motion, WASIM seems to induce a less displacement. For pitch motion, the mean rotation is close, but maximum rotation amplitude is larger in WASIM than the one in SIMO. It indicates the simulation from SIMO model tends to induce a larger response motion than the simplified quasi-static model, namely a more severe condition.

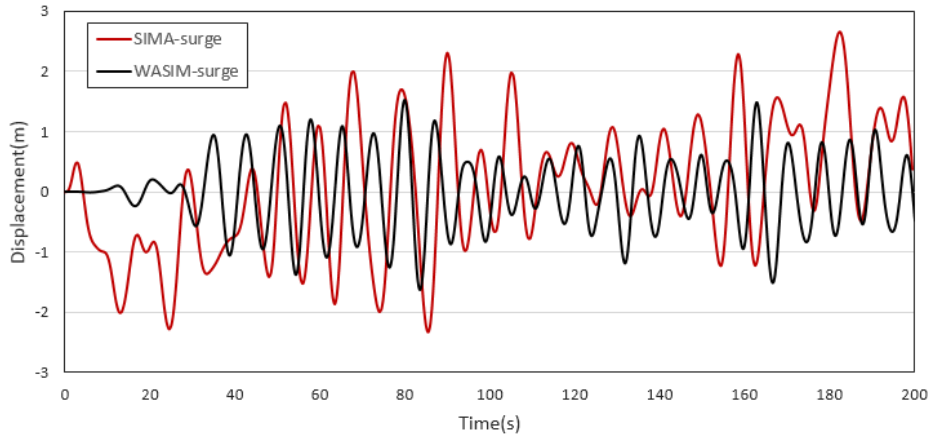

Figure 4.21: Comparison of surge motion simulated in Wasim and SIMA

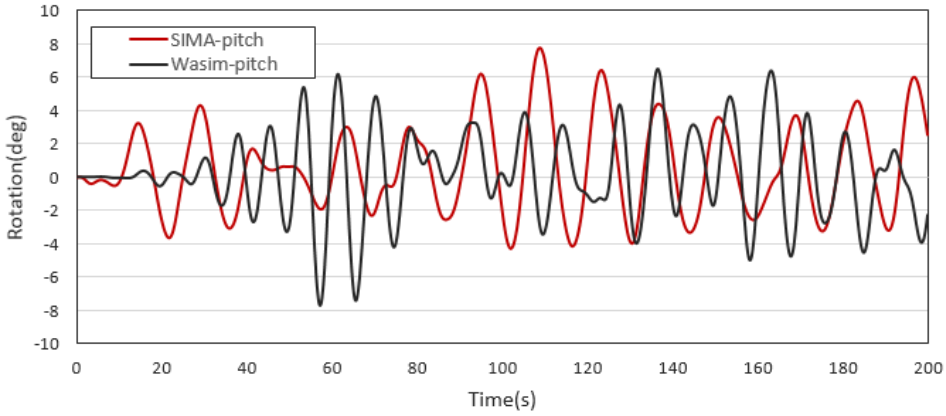

Figure 4.22: Comparison of surge motion simulated in Wasim and SIMA

Fig. 4.23 gives the Comparison between surge motion and wave elevation in catenary mooring system (SIMO) and linear spring element (WASIM) respectively. According to the graph, the model in SIMO acts the motion behind wave elevation with a phase of around 5s, while the delay is not observed in WASIM. In addition, the amplitude of WASIM surge motion shows to be limited under wave loads. In contrast, it is apparent that the motion in SIMO is relatively larger comparing with the wave elevation. The comparison reflects the effect of nonlinearity of mooring system, which leads to the response less in accordance with wave motion.

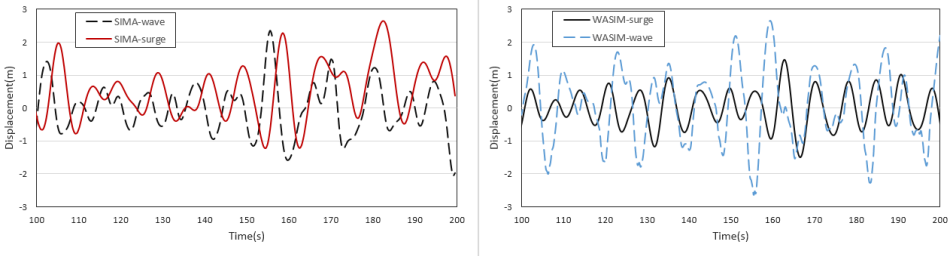

Figure 4.23: Comparison between surge motion and wave elevation in SIMA (right) and Wasim (left) respectively

Chapter 5

Conclusion and Further Work

5.1 Conclusion

The objective of this thesis was to study the feasibility of semi-submersible offshore fish farm in China East Sea. Therefore, dynamic response of the farm model was analyzed based on Chinese ocean condition. The analysis was carried out with numerical simulation program in both frequency and time domain.

The farm model was constructed based on the offshore farm "Ocean Farm 1", which is being operated in Norwegian sea. Some simplification was carried out at the design stage considering the actual situation in China. There are some components of the model: main body including central pontoon, net frame and connectors; fish nets; mooring system.

In order to calculate hydrodynamic properties of the farm structure, a composite model with both Morison beam and panel surface was constructed in GeniE. And simulating the composite model in WADAM, RAOs of response motion in six degrees of freedom are obtained. In addition, time domain analysis is carried out in WASIM program, and compared with the results of frequency domain analysis. It is observed that the response motions from time domain and frequency domain are generally similar. While for the amplitude in high frequency part, the response from time domain presents to be larger than frequency domain. The reason could be that the viscous damping in frequency domain is overestimated owing to stochastic lineariztion.

The kinetic results of farm acquired in WADAM were used as the input data of SIMO program to implement coupled analysis of mooring system in time domain. A catenary mooring system was modeled in SIMA to check its capability of keeping position in ultimate sea states. The hydrodynamic loads of fish nets were calculated through simplified Morison beam. In order to verify the feasibility of simplification, a sensitivity study in ABAQUS was conducted. There are 7 various environment conditions selected for the test according to the research of Zheng Kaiwen and Zhu Yanrong (Zheng et al., 2018; Zhu Yanrong, 1995). For the ultimate sea states, PM spectrum are applied with significant weight height $Hs = 4m$, wave period $T = 10s$.

For all of the simulations carried out in this thesis, the mooring lines presented to be capable of withstanding the hydrodynamic loads from waves and currents. None of the simulation lifted the mooring lines from the seabed from the view of dynamic animation, which means the mooring line capacity is sufficient for the farm structure. Moreover, the tension in mooring lines was also kept in an acceptable level and reached only 20% the maximum tension limit ($T_{max} = 1 * 10^6 N$).

Comparing the results of motion under different environment conditions, it indicates that current dominates drift motion of the farm other than wave drift force. The mooring line tension increased by 15% when a promotion of current velocity of 0.25 m/s is applied. However, when considering the oscillation motion of structure, wave force comes to be the main factor. Due to the symmetry of farm structure, wave from different direction only results in slight difference, and the effect of misalignment of wave and current is also insignificant.

Furthermore, mooring systems with different pre-tension are tested in a same environment. The results of simulation verifies that the pre-tension of mooring line has a non-linear effect on the drift of floating farm body. With the increasing of mooring line pre-tension, the performance of mooring system can be enhanced. Finally, the simplified quasi-static mooring system in WASIM is compared with the catenary mooring system in SIMO. And it illustrates the influence of nonlinear effects: the results from SIMO are less in accordance with wave motion.

5.2 Further Work

The dynamic analysis of offshore fish farm is complex and challenging. There are still lots of further work to be done in the future. The recommendations of further work are carried out based on the result of this thesis.

1. Experimental study could be carried out to compare with the results from numerical simulation. The verification of the numerical results is of great importance for practical application of the model.

2. In this thesis, only three mooring pre-tension are compared due to limitation of time. It is recommended that more pre-tension of the mooring lines could be tested to study the influence of pre-tension on offshore fish farm structure.

3. Instead of fully dynamic analysis, SIMO program is only capable of simplified dynamic analysis accounting the effect of drag force on the mooring lines. More accurate simulation might be carried on SIMO-Riflex for fully coupled analysis of mooring system.

Bibliography

AKSNES, V., 2016. Modelling of aquaculture net cages in sima. MARINTEK Report NT2016 F116.

Aqualine, 2019. Feeding technology.
URL https://aqualine.no/en/products/feeding-technology

Benitz, M. A., Schmidt, D. P., Lackner, M. A., Stewart, G. M., Jonkman, J., Robertson, A., 2014. Comparison of hydrodynamic load predictions between engineering models and computational fluid dynamics for the oc4-deepcwind semi-submersible. Tech. rep., National Renewable Energy Lab.(NREL), Golden, CO (United States).

Bjelland, H. V., Føre, M., Lader, P., Kristiansen, D., Holmen, I. M., Fredheim, A., Grøtli, E. I., Fathi, D. E., Oppedal, F., Utne, I. B., et al., 2015. Exposed aquaculture in norway. In: OCEANS 2015-MTS/IEEE Washington. IEEE, pp. 1–10.

Chakrabarti, S., 1987. Wave force on small structures. Hydrodynamics of offshore structures, Computational Mechanics Publications, Southampton, 168–170.

De Jong, P., 2018. TU Delft Open Course Ware. TU Delft.
URL http://links.giveawayoftheday.com/ocw.tudelft.nl/

DNVGL, 2017. DNVGL-RP-C205 Environmental conditions and environmental loads. DNV GL AS.

Faltinsen, O., 1993. Sea loads on ships and offshore structures. Vol. 1. Cambridge university press.

Fang, H., Duan, M., 2014. Offshore Operation Facilities: Equipment and Procedures. Gulf Professional Publishing.

FAO, 2018. The state of world fisheries and aquaculture 2018 - meeting the sustainable development goals.

Greco, M., 2012. Tmr 4215: sea loads lecture notes. Trondheim, Norway: Dept. of Marine Technology, Norwegian University of Science and Technology, 77–80.

Høiland, A. V., 2017. Dynamic analysis of a vessel-shaped fish farm for open sea.

HYDROD, D. S. U. M., 2006. Wave load & stability analysis of fixed and floating structures [g].

Lader, P. F., Enerhaug, B., 2005. Experimental investigation of forces and geometry of a net cage in uniform flow. IEEE Journal of Oceanic Engineering 30 (1), 79–84.

Lader, P. F., Enerhaug, B., Fredheim, A., Krokstad, J., 2003. Modelling of 3d net structures exposed to waves and current. In: 3rd International Conference on Hydroelasticity in Marine Technology. Department of Engineering Science, The University of Oxford Oxford, UK, pp. 19–26.

Lader, P. F., Fredheim, A., 2006. Dynamic properties of a flexible net sheet in waves and currenta numerical approach. Aquacultural engineering 35 (3), 228–238.

Larsen, K., 2014. Lecture note on Mooring and station keeping of floating structures. NTNU.

Larsen, K., Sandvik, P. C., et al., 2015. Fatigue analysis and design of mooring systems. Assessment and comparison of different methods. NTNU.

Larsen, K., S. P., 1990. Efficient Methods for the Calculation of Dynamic Mooring Line Tension. The First European Offshore Mechanical Symposium.

Li, L., Jiang, Z., Høiland, A. V., Ong, M. C., 2018. Numerical analysis of a vessel-shaped offshore fish farm. Journal of Offshore Mechanics and Arctic Engineering 140 (4), 041201.

Løland, G., 1991. Current Force on and Flow Through Fish Farms. Norwegian Institute of Technology.

Løland, G., 1993. Current forces on, and water flow through and around, floating fish farms. Aquaculture International 1 (1), 72–89.

Marintek, 2017. SIMO Theory Manual. Sintef.

Naess, A., Moan, T., 2013. Stochastic dynamics of marine structures. Cambridge University Press.

Newman, J., 1974. Second-order, slowly-varying forces on vessels in irregular waves. International Symposium on the Dynamics of Marine Vehicles and Structures in Waves, 182–186.

Nordlaks, 2015. Havfarm.
URL `http://www.nordlaks.no/Om-oss/Havfarm`

Ran, Z., Kim, M., Zheng, W., 1999. Coupled dynamic analysis of a moored spar in random waves and currents (time-domain versus frequency-domain analysis). Journal of Offshore Mechanics and Arctic Engineering 121 (3), 194–200.

Randall, R. E., 1997. Elements of ocean engineering. Society of Naval Architects and Marine Engineers.

Refamed, 2015. Tlc design.
URL http://www.refamed.com/gabbie_mare/tlc_system.html

Reinholdtsen, S., Falkenberg, E., 2001. SIMO user manual. Sintef.

Shao, Y.-L., You, J., Glomnes, E. B., 2016. Stochastic linearization and its application in motion analysis of cylindrical floating structure with bilge boxes. In: ASME 2016 35th International Conference on Ocean, Offshore and Arctic Engineering. American Society of Mechanical Engineers, pp. V001T01A016–V001T01A016.

Sunde, L. M., Heide, M. A., Hagen, N., Fredheim, A., Forås, E., Prestvik, Ø., 2003. Teknologistatus i havbruk. SINTEF Fiskeri og havbruk. Report number: STF80 A 34002.

Terazono, E., 2017. Norway turns to radical salmon farming methods.
URL https://www.ft.com/content/a801ef02-07ba-11e7-ac5a-903b21361b43

Tnset, M., 2017. Snart klar for 1,6 millioner laks.
URL https://www.adressa.no/nyheter/okonomi/2017/09/15/Snart-klar-for-16-millioner-laks-15312949.ece

Veritas, D. N., 2010. Dnv-rp-c205: Environmental conditions and environmental loads. Det Norske Veritas: Oslo, Norway.

Zhang, F., Yang, J.-m., Li, R.-p., Gang, C., 2008. Coupling effects for cell-truss spar platform: comparison of frequency-and time-domain analyses with model tests. Journal of Hydrodynamics, Ser. B 20 (4), 424–432.

Zheng, K., Osinowo, A. A., Sun, J., Hu, W., 2018. Long-term characterization of sea conditions in the east china sea using significant wave height and wind speed. Journal of Ocean University of China 17 (4), 733–743.

Zhu Yanrong, Xie Jun, G. P., 1995. Research on applicability of various wave spectra in ocean engineering. Acta Oceanologica Sinica 17 (6), 126–131.

Appendix A

Comparison of pitch RAOs with different frequency set

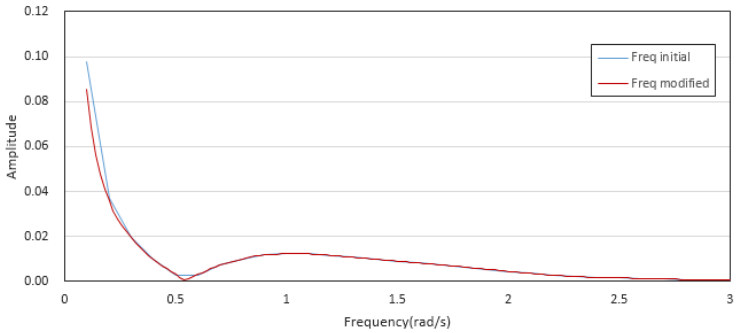

Comparison of roll RAOs with different frequency set

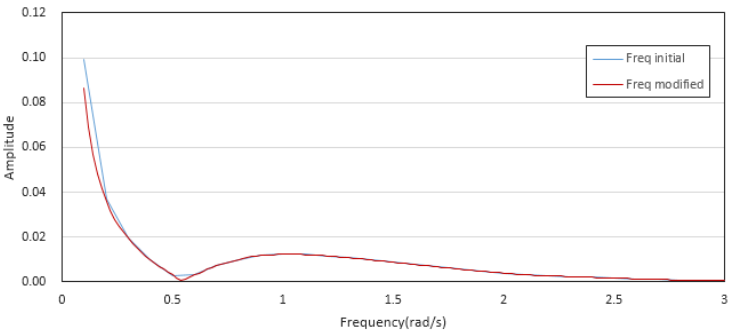

Appendix B

MATLAB code for mooring static calculation:

```
% Water depth is set to be 100 meters
h = 0:1:100;

% Horizontal load [N]
% Pre-angle is 35 degrees and Pre-tension is 120 kN
phi = 35; T_pret = 120000;
H = T_pret*(sind(phi)) ;

% Submerged weight per meter [N/m]
Ws = 71*9.8 ;

% Distance to touchdown point [m]
L = (H/Ws)*acosh(((Ws*h)/H)+1);
indexmax = find(max(L) == L);
Lmax = L(indexmax);

% x is used as lenght for further calculations
x = L;

% Geometric profile of catenary
y = (H/Ws)*(cosh((Ws/H)*x)-1);
y_max = (H/Ws)*(cosh((Ws/H)*Lmax)-1);

% Distance from touchdown point to anchor
s = (H/Ws)*(sinh((Ws*Lmax)/H)) ;
d=250-s;
x2 = -d:1:0;
indexmax2 = find(max(x2) == x2);
y2 = zeros(1,indexmax2);

% Coordinates of touchdown point
x_td = 0;
y_td = 0;

% Plot mooring line geometry figure
plot(L,y,'b');
grid on;
hold on;
plot(x2,y2,'b');
```

```
hold on;
plot(x_td,y_td,'ro','MarkerSize',13);
axis tight;
xlabel('Distance from touchdown point [m]');
ylabel('Distance to seabed [m]');
title('Catenary geometry');


s = (H/Ws)*(sinh((Ws*Lmax)/H)) ;

%Tension
T = sqrt((H^2)+(Ws*s).^2);

% Vertical load [N]
V = Ws*s ;

%Max tension
Tkg = T/10;
```

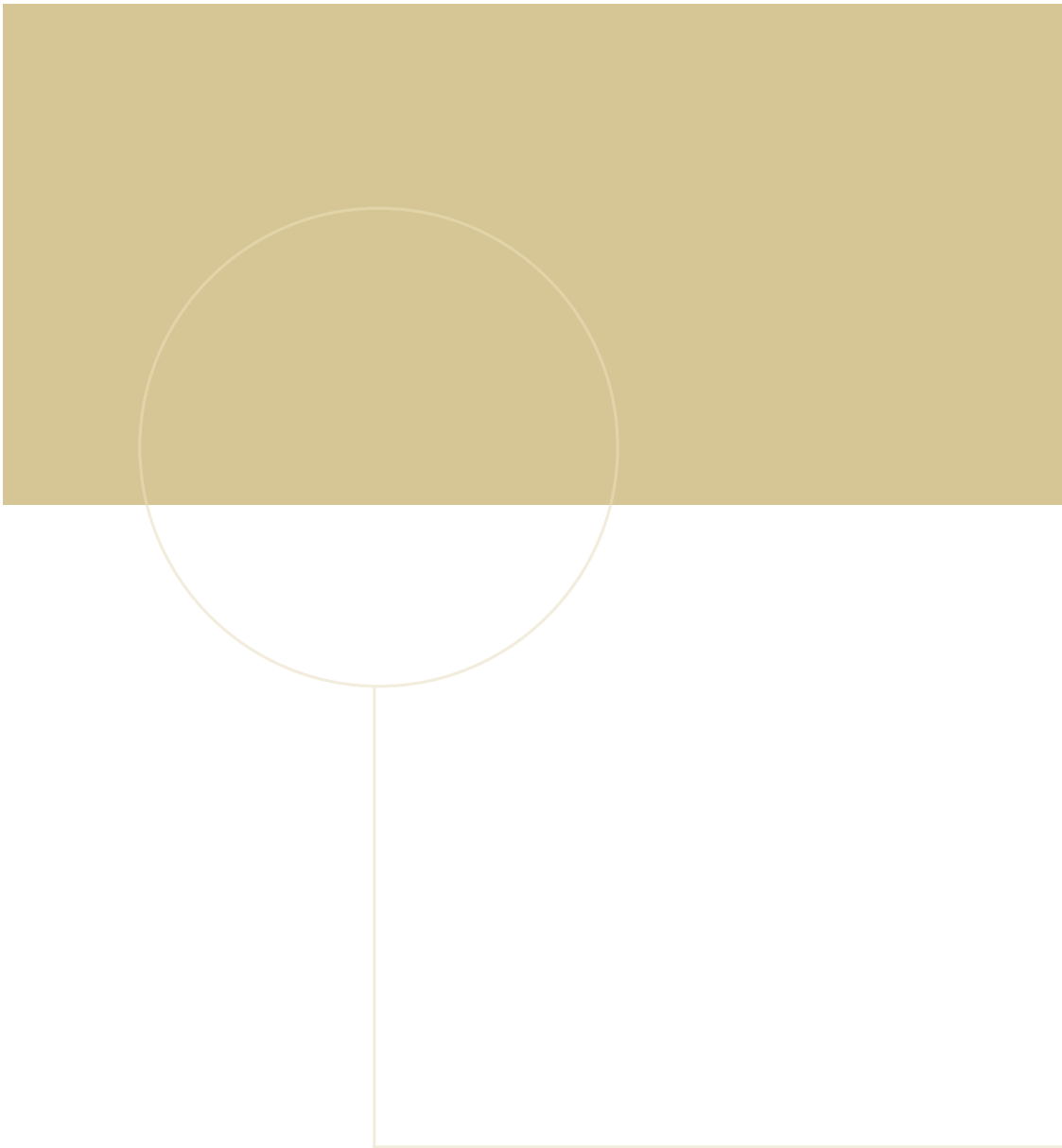

NTNU
Norwegian University of
Science and Technology